Universidade do Minho
Escola de Engenharia

Joana Filipa Ferreira de Matos

Development of a 3D multibody
system of the human lumbar spine

outubro de 2013

Universidade do Minho
Escola de Engenharia

Joana Filipa Ferreira de Matos

Development of a 3D multibody
system of the human lumbar spine

Tese de Mestrado
Ciclo de Estudos Integrados Conducentes ao
Grau de Mestre em Engenharia Biomédica

Trabalho efetuado sob a orientação do
Professor Doutor José Carlos Pimenta Claro
Professor Doutor João Paulo Flores Fernandes

outubro de 2013

DECLARAÇÃO

Nome: Joana Filipa Ferreira de Matos

Endereço electrónico: a58516@alunos.uminho.pt   Telefone: +351 918 735 292

Número do Bilhete de Identidade: 13658870

Titulo dissertação: Development of a 3D multibody system of the human lumbar spine

Ano de conclusão: 2013

Orientadores: Professor Doutor José Carlos Pimenta Claro

Professor Doutor João Paulo Flores Fernandes

Designação do Mestrado: Ciclo de Estudos Integrados Conducentes ao Grau de Mestre em Engenharia Biomédica

Área de Especialização: Biomateriais, Reabilitação e Biomecânica

Escola: de Engenharia

Departamento: de Engenharia Mecânica

Universidade do Minho, ___/___/_____

Assinatura _____

Acknowledgments

Throughout the development of this work, there were people who have demonstrated quite helpful and always available for me.

It is essential to acknowledge my supervisor, José Carlos Pimenta Claro and João Paulo Flores Fernandes, for giving me this opportunity, for the guidance, for always been available and for all the support and help throughout this work.

I acknowledge the support of the European Project: *NP Mimetic – Biomimetic Nano-Fiber Based Nucleus Pulposus Regeneration for the Treatment of Degenerative Disc Disease*, founded by the European Commission under FP7 (grant EU246351/CT2M-MSc06).

My acknowledgment for all the collaborators of CT2M – Centre of Mechanical and Materials Technologies, especially to Carina Lourenço, Tiago Correia, Clara Cavalcanti, Sara Cortez and André Castro for always been available for my doubts.

Finally, a special thanks you to my family and friends for all the encouragement and support through these years.

Abstract

Development of a 3D multibody system of the human lumbar spine

In the present work, a three-dimensional multibody model of the lumbar spine was developed to analyse the force and torques that each intervertebral disc (IVD) is subjected during daily movements.

The first work's stage summarizes the literature review of the state-of-the-art of the multibody models of the spine. It was also characterized the anatomy of the spine, detailing at the vertebrae of the lumbar spine and sacrum, the facet joints, the intervertebral disc and the ligaments.

The model is composed by five intervertebral discs, six vertebrae (L1 to S1), ligaments and facet joints. The vertebrae were simulated as rigid bodies, the intervertebral discs as bushing elements (with six degree-of-freedom), the ligaments as spring elements and the facet joints as separators. The spring constant of the bushing elements were characterized using data from a Finite Elements dedicated software, developed under the research project in which this work is inserted. To characterize the spring constant of the ligaments a curve of force-deformation found in the literature was used.

After the model validation (with data found in the literature), it was possible to see how the force/torque is distributed along the intervertebral discs during several simulated movements: flexion, extension, lateral bending, axial rotation, traction and compression.

Besides a healthy lumbar spine, it was also simulated a spine with fusion of L4L5 to calculate the percentage of variation of the force/torque that each IVD is subjected comparing with the healthy spine.

Key-words: multibody systems, lumbar spine, intervertebral disc, bushing element, movement analysis

Resumo

Desenvolvimento de um modelo multi-corpo 3D da coluna lombar humana

No presente trabalho, um sistema multibody tri-dimensional da coluna lombar foi desenvolvido com o objetivo de analisar as forças e momentos a que cada disco intervertebral está sujeito durante movimentos diários.

A primeira etapa do trabalho consistiu no resumo do estado-de-arte dos modelos multibody da coluna vertebral. Também foi caracterizada a anatomia da coluna vertebra, detalhando as vértebras da coluna lombar e o sacro, as facetas, o disco intervertebral e os ligamentos.

O modelo é composto por cinco discos intervertebrais, seis vértebras (L1 até S1), ligamentos e facetas. As vértebras foram simuladas como sendo corpos rígidos, os discos intervertebrais como sendo *bushing elements* (com seis graus-de-liberdade), os ligamentos como sendo mola e as facetas como sendo separadores. As constantes de mola dos *bushing elements* foram caracterizadas usando dados gerados por um método de elementos finitos dedicado, no âmbito do projecto mais vasto em que este trabalho está inserido. Para caracterizar a contante de mola dos ligamentos usou-se curvas de força-deformação encontradas na literatura.

Depois da validação do modelo (com dados encontrados na literatura), usou-se este para analisar a forma como os esforços (forças e momentos) se distribuem ao longo dos discos intervertebrais durante os movimentos simulados: flexão, extensão, rotação lateral, rotação axial, compressão e tração.

Além da coluna saudável, também foi simulada a coluna vertebral com fusão L4L5 para a calcular a percentagem da variação da força/momento a que cada disco intervertebral está sujeito comparativamente com a coluna saudável.

Palavras-chaves: sistemas multibody, coluna lombar, discos intervertebrais, análise movimento.

Contents

List of Abbreviations and Acronyms

3D: Three-Dimensional

AF: Annulus Fibrosus

ALL: Anterior Longitudinal Ligament

CL: Capsular Ligament

FE: Finite Element

ISL: Interspinous Ligament

IVD: Intervertebral Disc

LF: Ligamentum Flavum

PLL: Posterior Longitudinal Ligament

MBS: Multibody System

MRI: Magnetic Resonance Image

NP: Nucleus Pulposus

SSL: Supraspinous Ligament

VBR: Vertebral Body Replacement

WM: Working Model

List of Figures

List of Tables

Chapter 1 - Introduction

1.1. Motivation and Scope

Musculoskeletal conditions are the most common cause of severe long term pain and disability and lead to significant healthcare and social support cost. Low back pain is one of the most common musculoskeletal disorders in the world and it's a major health and socioeconomic problem in Europe. It can lead to reduced physical activity, lost wages, diminished quality of life, and psychological distress affecting seriously the quality of life of those with the condition and that of their families, friends and careers (1).

At some point of their lives, 70% to 80% of individuals experiences low back pain. In children and adolescents, the prevalence ranges between 11% and 50%. In adulthood, the prevalence ranges between 60 to 80%, where in adults less than 45 years old, this condition is the most common cause of disability, but only 2 to 15% will look for medical advice (2).

The total costs of low back pain in the USA exceed $100bilion per year. Two-third of these cost are indirect, due to lost wages and reduced productivity. The direct costs are related with direct medical care (3). In Portugal, according with the Portuguese Magazine of Public Health, the indirect costs with chronicle back pain, in 2010, was €738.85 million, of which €280.95 million was because of absenteeism generated by short-term inability and €458.90 million due to the reduction of employment for early retirements and others forms of non-participation in the labor market (4).

There are many causes for the low back pain, and the degeneration of the intervertebral disc is pointed as the most common cause. With this in mind, the objective of this work is to develop a 3D multibody system of the human lumbar spine, using data from a Finite Element dedicated software, developed under the research project in which this work is inserted, for the study of the behavior and solicitations that each intervertebral disc is subjected during daily movements.

1.2. Literature Review

The mathematical models are used to simulate biological and they are undoubted advantageous because it can simulate situations in which others means of investigations are not feasible, they are more economical and safer. With the use of high-speed modern computer, such models, once validated by experiments and clinical application, can become a powerful tool to understanding, prevention and treatment of spinal disorders. About the computational models, there are two methods used to simulate the human spine: multibody system and finite element method. A multibody system consisted of rigid bodies connected through kinematic joints and elements applying forces. On the other hand, finite element systems are able of producing highly detailed models of bodies and systems by dividing the entities into a number of smaller elements, connecting those via nodes, and producing the realistic material behavior by employing governing FE equations. Multi-body dynamics models have advantages such as less complexity, less demand on computational power, and relatively simpler validation requirements when compared to FE models (5) (6).

In 1957, Latham was the first to publish an analytical model of the spine, with the objective of studying pilot ejections. During the 1960's the model was improved adding dampers and more degrees-of-freedom to represent the vertebrae and IVDs (7).

Orne and Liu presented a more realistic model in 1970, to study the spinal response to impact. In their model they considered the internal stress, forces of shear and bending that act on the disc, and also the viscoelastic behavior of the IVDs (7).

A three dimensional FE model of the spine was developed by Belytschko and his co-workers in 1978 to evaluate the mechanical response of a pilot during ejection. The model was composed by all the vertebrae and the head as rigid bodies. The ligaments and the muscles were modeled as springs (7).

In 1981, Merril presented a model consisted of the head, cervical and thoracic vertebrae that were connect by spring and hysteretic elements. The muscles also were represented as linear elements (8).

Williams and Belytschko developed, in 1983, a three dimensional human cervical spine model for impact simulation. The cervical vertebrae and the head are modeled as rigid bodies which are interconnected by deformable elements representing the IVDs, facet joints, ligaments and

muscles. The novelty of their model was the special pentahedral continuum element that represents the facet joint. In that way, the model is able to simulate both lateral and frontal plane motion (9).

Shirazi and his co-workers constructed a general three-dimensional finite element for the analysis of the lumbar intervertebral disc L23 in 1984. The geometry of the model was based on *in vitro* measurements and the discs were represented by non-linear properties of its elastic elements. They simulated a normal and degenerated disc under compressive forces (7) (10).

In 1984, Deng and Goldsmith defined a numerical model for predicting sagittal-plane motion of the human head-neck during impact. The model was composed by human cervical and thoracic vertebrae, assumed as rigid bodies that were interconnected by intervertebral joints, and also fifteen pairs of muscles, represented as linear elements (8).

Jaeger and Luttamann presented a three-dimensional dynamic biomechanical human model in 1989 which allows to quantifying torque, compressive and shear forces, and pressure at the lumbar IVDs during various trunk flexions. Their model was compound by 19 body segments, where the vertebrae were represented as rigid bodies, the IVDs as linear viscoelastic elements, the ligament as nonlinear viscoelastic elements, and it was also constituted by facet joints and contractile muscle elements. To validate their model they compared their results with the intradiscal pressure measurements taken form the literature (9).

Figure 1.1 – Three-dimensional dynamic biomechanical human model developed by Jager and Luttmann with 19 body segments {Adapted from (6)}.

Monheit and Badler developed, in 1990, a kinematic model of the human spine and torso based on the anatomy of the physical vertebrae and discs, the range of movement of each

vertebra and the effect of the surrounding ligaments and muscles. To construct the model, they used the Jack software system that was developed at the University of Pennsylvania for human figure modeling and manipulation (11) (9).
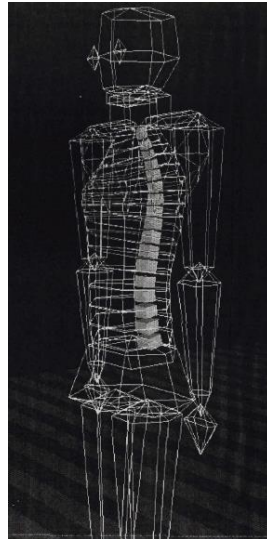
Figure 1.2 - Representation of the model developed by Monheit and Badler {Adapted from (11)}.

In 1992, Lavaste and Jones presented a three-dimensional finite element model of the lumbar spine. They based the model's geometry, on eight cadavers, using X-rays and digitizers to facilitate the model validation. To connect vertebrae they used intervertebral disc and ligaments. This last one was represented by a line that attaches two points of adjacent vertebrae (12) (7).
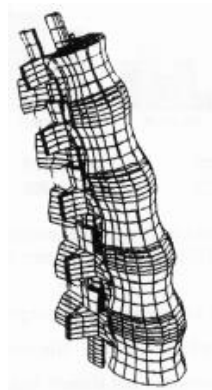
Figure 1.3 - Finite Element model of the lumbar spine developed by Lavaste and Jones {Adapted from (7)}

Menon developed a mathematical model of a human head-neck-torso system in 1995. The model was used to simulate real crash situations, to study the dynamic response and injury mechanism. The head and the vertebrae (7 cervical and the first thoracic) were represented as rigid bodies. The muscles, intervertebral discs, cartilage, ligaments and others components were

characterized as non-linear rotational spring dampers. To validate the model they compared their results with the results obtained using volunteer subjects (13) (14).

In July of 1996, Broman and his co-workers published an article that describes a mathematical model of the lumbar spine, pelvis and buttocks to study the influence of vibrations from the seat to L3, of individuals, in the sitting posture. Their strategy passed through to consider the skeletal system as rigid. The soft tissue was modeled as linear components (15) (9).
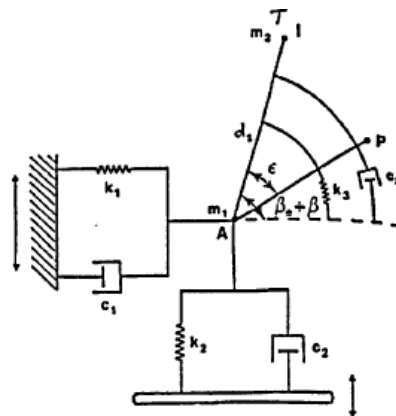
Figure 1.4 - Modeling components from the work of Broman and co-workers {Adapted from (6)}

A study of Kitazaki and Grifin, in 1997, presented a two-dimensional model capable of predicting the biomechanical effect of vibrations in the lumbar spine, using the finite element method. To model the spine, head, pelvis and soft tissues (buttocks and viscera) they used beams, springs and mass elements. To validate their model, they compared the result with the ones measured in their laboratory (16) (17).
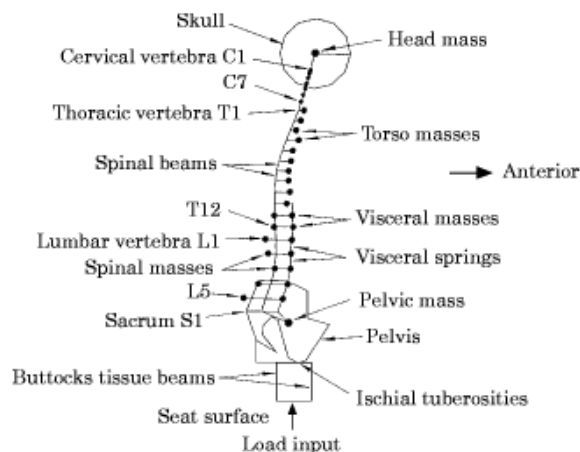
Figure 1. The two-dimensional biomechanical model in the normal posture.

Figure 1.5 - Representation of the two-dimensional biomechanical model (and his components) developed by Kitazaki and Grifin {Adapted from (16)}

In 1998, an article published by Pankoke and his co-workers, describes a dynamic finite element model of a man sitting to calculate internal forces in the lumbar intervertebral discs. They incorporated the L3, L4 and L4 vertebrae into a dynamic model with neck/head, arms, pelvis and legs. A simple dynamic representation of the viscera at the lumbar spine was used. The back muscles, ligaments, intervertebral discs, articulating process (L5-S1) and others interconnecting bodies were modeled as linear springs. The stiffnesses of the spine model used static *in vitro* experiments found in the literature. To validate the complete model's dynamic behavior, they compared their results with measurements found in the literature. The results were considered satisfactory to predict the active inertial forces and the dynamic behavior of the lumbar spine (18) (17).
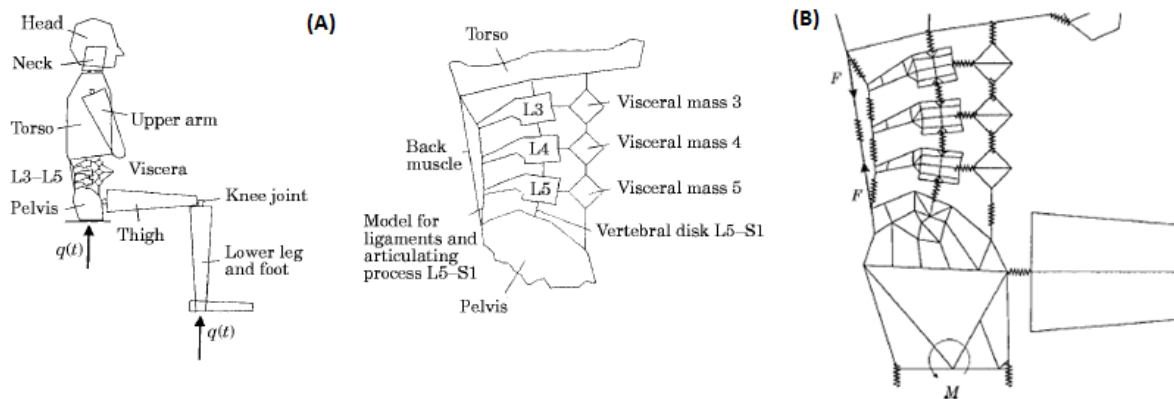
Figure 1.6 - Representation of the model developed by Pankoke and co-workers. (A) The complete model and the detailed lumbar region. (B) Simulation of the muscles, ligaments, IVDs and articulating process as spring {Adapted from (18)}

In 1999, Stokes and his co-workers developed a rigid model to study the muscles and spinal forces. The model included five lumbar vertebrae, twelve thoracic vertebrae, the sacrum and sixty-six muscles. The bony anatomy was based on standing stereo-radiographs of four young healthy adults. They created two models with the same geometry, but with different properties: the stiffness model (where the vertebrae as beams with predetermined stiffness properties) and the static model (where the vertebrae were interconnecting by 'ball-and-socket' joint). Both models were subjected to flexion, extension, lateral bending and axial torque tests (19) (7).
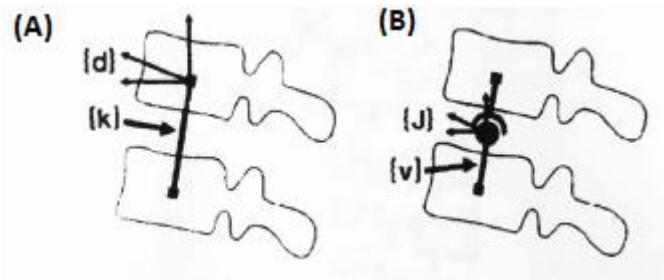
Figure 1.7 - Representation of the two models developed by Stokes and his co-workers. (A) Model with stiffness. (B) Model without stiffness {Adapted from (19)}

De Jager presented, in 2000, a detailed three dimensional mathematical head-neck model to study the human responses to impacts. His final model integrated a rigid head and vertebrae, linear viscoelastic discs, frictionless facet joints, nonlinear viscoelastic ligaments and segmented contractile muscles. To validate the model they used human volunteer responses. They concluded that the muscles are an essential element to describe the human head-neck response to impact. The detailed model is suitable for studying neck injury mechanism and neck injury criteria (20) (14) (8).
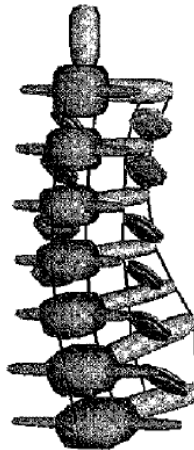
Figure 1.8 – Partial representation of the model developed by Jager {Adapted from (20)}.

Lengsfeld and his co-workers constructed a mathematical model, using the ADAMS® software, to study the lumbar spine curvature during office chair sitting. The model consisted of fifteen rigid segments, where four segments represent the pelvis, thigh, leg and foot. The hip was modeled as a spherical joint. The lumbar vertebrae were modeled according with the geometrical data found in literature. The IVDs were modeled as revolute joint simulating flexion and extension movement. The model was developed to test lumbar spine curvature of two office chairs (21) (7).
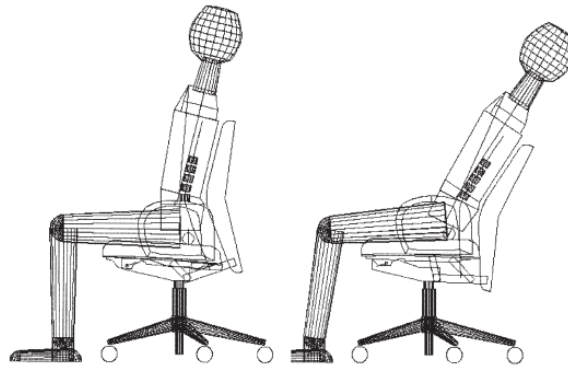
Figure 1.9 – Wire-frame representation of the model developed by Lengsfeld and co-workers during office chair sitting {Adapter from (21)}.

In 2002, Lopik validated a three dimensional multibody model of the human head and neck. The head and the 7 vertebrae of the neck were modeled as rigid bodies, interconnected by linear viscoelastic intervertebral discs, nonlinear viscoelastic ligaments, frictionless facet joints and contractile muscle. To modeled, they used the dynamic simulation package MSC.visualNastran 4D (9).
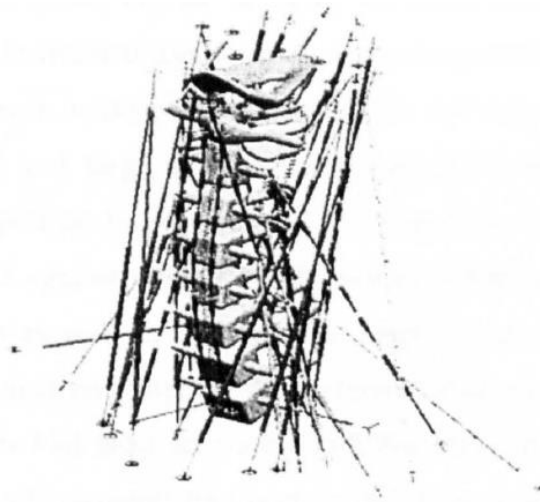
Figure 1.10 - Representation of the cervical spine model with all the musculature developed by Lopik [Adapter from (6)}.

Keller and Colloca presented, in 2002, an article that study the kinematic response of the lumbar spine to static and dynamic posterioranterior forces used by clinicians during treatments. For that, they developed a two-dimensional model analysis capable to predict the dynamic motion response of the lumbar spine. The model had five degree of freedom; the lumbar vertebrae were modeled as masses that were interconnected by spring-dampers elements; the thorax and sacrum are assumed to be immobile. The motion of lumbar spine was calculated using differential equation (22) (7).
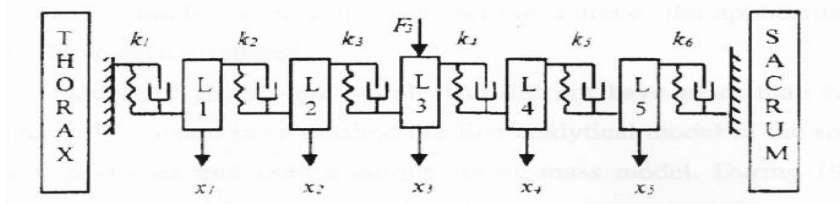
Figure 1.11 - Model lumbar spine developed by Keller and Colloca with 7 rigid bodies and 6 IVDS (spring-dampers elements) {Adapted from (7)}

Mark de Zee and his co-workers presented, in 2003, a detailed multibody lumbar spine model using the AnyBody Modelling System software. The model consisted into five rigid lumbar vertebrae, one rigid segment as pelvis and another rigid segment as a thoracic part, with eighteen degrees of freedom and one hundred and fifty four muscles. The rigid bodies were interconnected by spherical joints with three degrees of freedom. The vertebrae and muscle geometry was based on data from the literature. To predict the muscle and joint reaction forces, an inverse dynamic analysis was used. Their validation was limited to the maximum extension moment during upright standing postures by comparing the intradiscal pressure with the *in vivo* measurement found in the literature (9) (6).
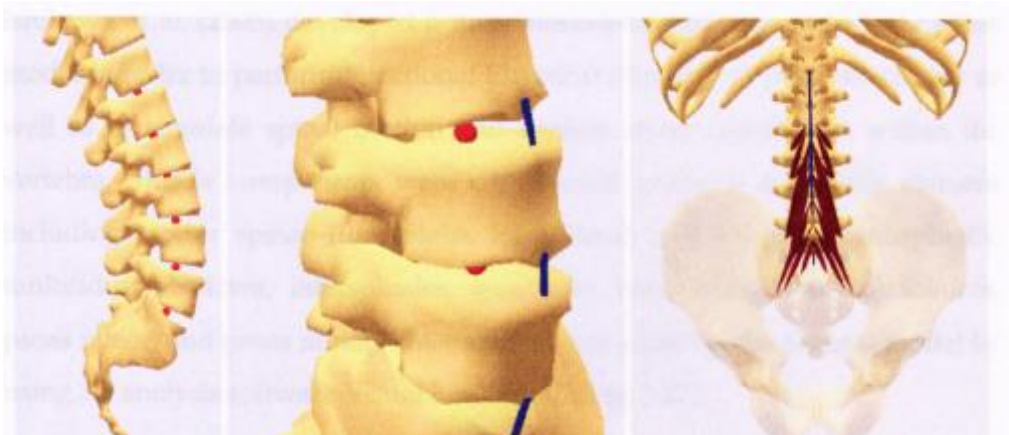
Figure 1.12 - Several views of the model developed by Mark de Zee and co-workers with the representation of the IVDs (red spherical joints), ligaments (blue segments) and lumbar muscles (red segments) {Adapted from (6)}

In 2003, Waters and his co-workers wrote a paper that describes the development a multibody model for the assessment of the risk of low back disorders due to occupational exposure to jarring and jolting from operation of heavy mobile equipment. The model consisted into four rigid elements connected by three spring-damper elements. Each rigid body represents the seven cervical vertebrae, the twelve thoracic vertebrae, the five lumbar vertebrae and the sacrum. The intervertebral discs were modeled as spring-damper element (23) (14).
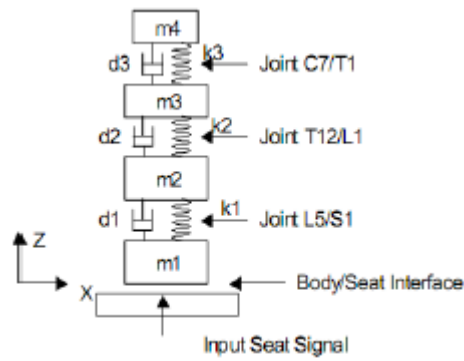
Figure 1.13 – Multibody model of the human spine developed by Waters and his co-workers {Adapted from (14)}.

Ishikawa and his co-workers published an article in 2005 that describes a musculoskeletal dynamic model of the spine that could perform Functional Electrical Stimulation properly and also that could simulate the spine motion and analyses the stress distribution within the vertebrae. The geometry of the skeletal was based into computed tomography data of one young health man volunteer. The muscles were joined to the skeletal model by using 3D analysis software Nastran 4D. The intervertebral discs and ligaments were modeled as spring-damper elements. To simulate the dynamic of the spine and to analyses the stress distribution, they used the 3D analysis software 'Visual Nastran 4D' (24) (9).
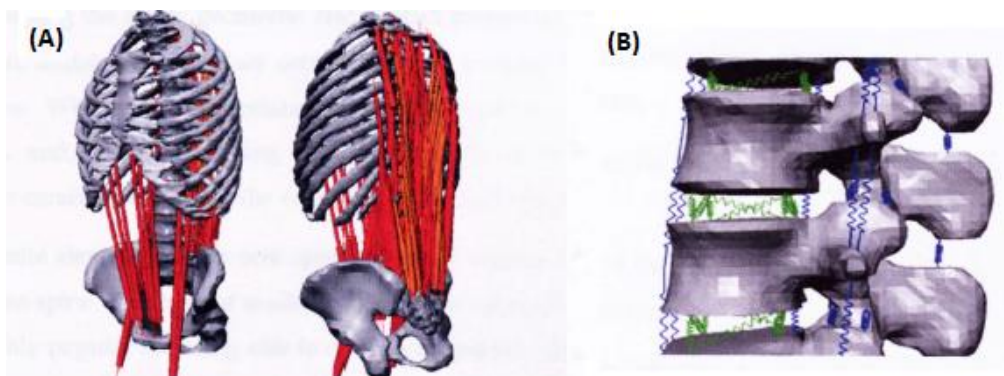
Figure 1.14 – Representation of the model developed by Ishikawa and co-workers. (A) General view. (B) Detailed representation of the IVDs and ligaments in the model {Adapted from (6)}.

Esat developed and validated a hybrid model of the whole human spine and it components to analyses the responses of the intervertebral discs under complex dynamic loading occurring during impact situations. The model was built using the dynamic simulation package visualNastrans 4D 2001. He considered four elements of the human spine: the vertebrae, the muscles, the ligaments and the intervertebral discs. The muscles were modeled as contractile muscle element, the ligaments as nonlinear viscoelastic elements and the intervertebral discs as bushing elements. The values used for the ligament's stiffness were from the work of Pintar.

About the damping coefficients of the IVDs, for translational was 1000 kg/s and for rotational was 1.5Nm/s. The IVDs stiffness data was based on the Gardner-Morse and Stokes's work. To validate the MBS, he compares the flexion moment result and the intradiscal pressure after the loading with a previously validated work of Shirazi-adl (6).
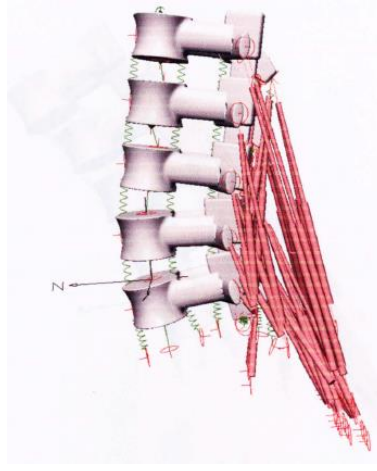
Figure 1.15 – Multibody system of the lumbar spine developed by Esat with four elements: vertebrae, IVDs, ligaments and muscles using the visualNastrans 4D 2001 software {Adapted from (6)}.

In September 2008, Ferreira presented a tridimensional model of human head and neck. The model consisted into the head, seven cervical vertebrae, the first thoracic vertebrae, six intervertebral discs and thirty one cervical ligaments. The intervertebral discs were modeled as bushing elements, the ligaments as nonlinear viscoelastic elements and the other components as rigid bodies. He also considered the bony contacts as a sphere-plane contact with nonlinear forces. The anatomy and mechanical properties of the cervical elements were based on data found in the literature. To validate the model, he compares the predicted result from his model with the values found in the literature for the segments range of motion in response to several loads (25) (14).
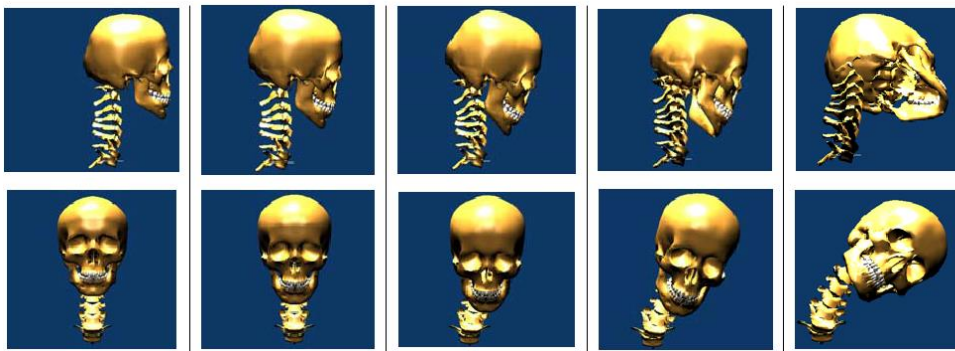
Figure 1.16 –Representation of the sagittal and frontal view of model during the lateral impact developed by Ferreira {Adapted from (25)}.

Zhang and Teo published a paper in 2008 that describes a finite element model that could lean the research field of implants for low back pain treatment. The model predicted the values of stresses in the disc, vertebrae and ligaments. It also provides a detailed motion data of the segments (26) (7).

In 2009, Nuno Monteiro developed a co-simulated model of a multibody system dynamic and finite element model to study the cervical and lumbar spine dynamics in a pathologic situation (intersomatic fusion between one or more spine levels). The cervical and lumbar model consisted, respectively of nine (C1-T1) and six (L1-S1) vertebrae, forty nine and thirty five ligaments and twenty three and fifteen contacts corresponding to the articular facets and the contact between the spinous processes. The vertebrae were modeled as rigid bodies, the intervertebral discs as linear viscoelastic bushing elements, the ligaments as nonlinear elastic springs and the spinal contacts model was based on the nonlinear Kelvin-Voigt contact model. To validate the model he compares his results with the data found in the literature (8) (14).

Fairman and his co-workers proposed, in 2009, a multibody model of the lumbar spine to predict the joints kinetics during complex activities. The vertebrae geometry was simplified (elliptical bodies). The joints were modeled as spring-damper elements and they represented the IVDs and the ligaments. They also represented the muscles as actuators. They used the MATLAB simulation tool Simulink to develop the MBS (27) (14).
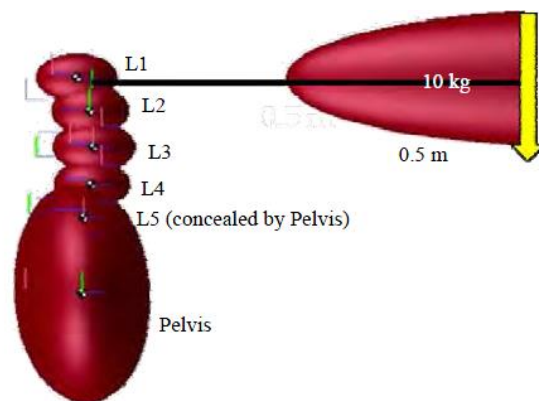
Figure 1.17 –Multibody model of the lumbar spine, under a loading situation, developed by Fairman and co-workers {Adapted from (27)}.

In 2009, Juchem created a three dimensional multibody system to calculate the transmitted forces and torques in the bony and elastic structures of the lumbar spine. The model consisted into four rigid lumbar vertebrae and a rigid sacrum. Between the rigid bodies, there was elastic elements representing the IVDs, and the contact from facet joint and the ligaments also were

added into the model. Their geometry was based in data from computer tomography measurements. While an external force was acting on the top of L2, the model was able to calculate the forces and torques in each IVD and also the forces in the ligaments (28) (14).

Figure 1.18 – Three dimensional model of the lumbar spine developed by Juchem with 5 rigid bodies, IVDs, ligaments and facet contact {Adapted from (14)}.

Roozbeth Seradj-Zadeh developed and validated a multibody computational model of the lumbar spine to predict joint reaction forces and torques, muscle forces and others parameters. The model comprises the five lumbar vertebrae and the pelvis, all of them was modeled as rigid bodies. The geometry dimensions were based on data found in the literature. To connect the bodies, he modeled the IVDs as kinematic and dynamic constraints, which allows a six degree of freedom. Some ligaments (supraspinous, interspinous, intertransverse) also were modeled as spring elements. The torque caused by the muscle forces were implemented by using torque actuators between the rigid bodies. The validation passes through compare the result from the MBS with an experimental study with a human volunteer (7).
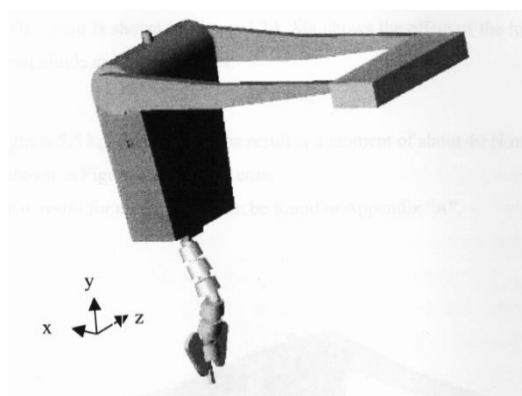
Figure 1.19 – Multibody computational model developed by Zadeh with 11.5 kg weight applied {Adapted from (7)}.

Chen studied the effect of the vertebrae fusion by calculating the stress distribution of the intervertebral disc with a finite element model of the lumbar spine. They compare three

situations: healthy lumbar spine; a lumbar spine with a pair of bilateral posterior lumbar interbody fusion with also screw implant in the pedicle of L3 and L4; and a lumbar spine with disc prosthesis (ProDiscll) at L3-L4. They simulated various loading conditions: flexion, extension, lateral bending and torsion (29) (7).

In 2010, Christophy focused his work on the effect of the muscles in the spine motion. With that purpose, he developed a musculoskeletal model of the lumbar spine. Besides the skeleton, the model also represented the IVDs and the muscles. The IVDs were modeled as a joint with six degrees of freedom; and the muscles follow the Hill-type and the Thelen's muscle models (30) (14).
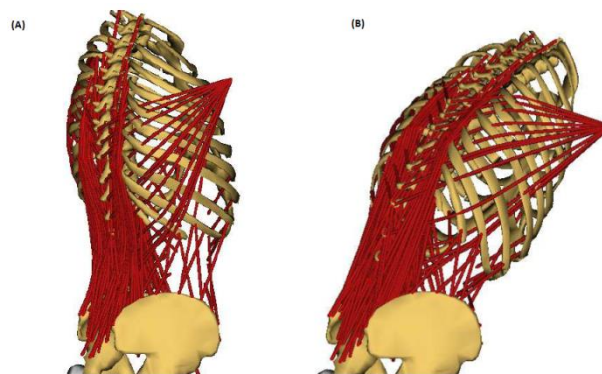
Figure 1.20 – Musculoskeletal model developed by Christophy, with 238 muscles, 13 rigid bodies and 5 intervertebral bodies. (A) Neutral posture. (B) 50◦ flexion {Adapted from (30)}.

Abouhosein and his co-workers published in 2010 an article that described a three dimensional multibody of the lumbar spine to determine loading sharing between the passive elements. The model consisted of six rigid bodies of the human lumbosacral spine (five lumbar vertebrae and sacrum), IVDs (modeled as nonlinear flexible element with six degree of freedom), ligaments (simulated as tension-only force elements) and the facet contact. The model was constructed using MSC.ADAMS ® dynamic software. To validate their model, they compare their prediction for the kinematic and facet joint forces, in response to pure torque loading with *in vitro* data (31) (14).
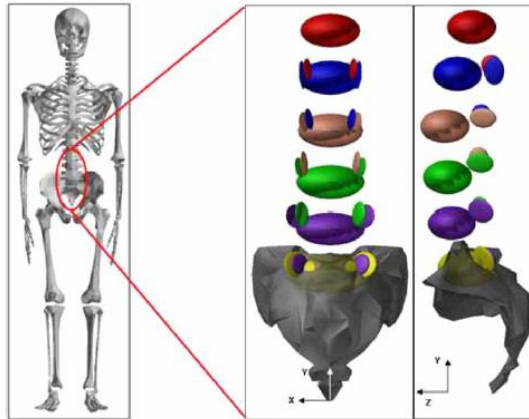
Figure 1.21 – Lumbosacral spine model developed by Abouhosein and co-workers, without the representation of the constraints and connectors {Adapter from (31)}.

Sara Morais developed in 2011 a two dimensional lumbar spine model using the FORTRAN code MUBODYNA. The model consisted in six rigid bodies (5 lumbar vertebrae and sacrum) interconnected by linear viscoelastic bushing elements as IVDs and nonlinear viscoelastic elements as ligaments. She also simulated the contact between the facet joint and spinous processes, following the hertzian contact theory augmented with dissipative term. To validate the model, an individual validation of the methologies was made (14).
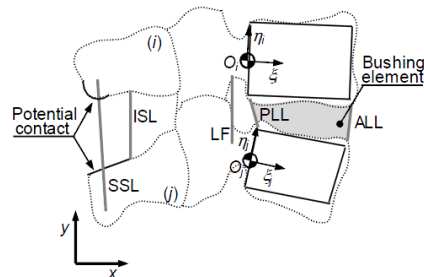
Figure 1.22 – Representation of the two dimensional lumbar spine model developed by Morais, using the finite element method {Adapted from (14)}.

Galibarov et al developed in 2011 a computational approach for investigating effect of muscular and external forces on curvature of the lumbar spine. The model of the lumbar spine was from the Anybody Modelling System software. The ligaments and the IVDs of the lumbar spine were added. The IVDs were modeled as spherical joints positioned in the instant centers of rotation (32).
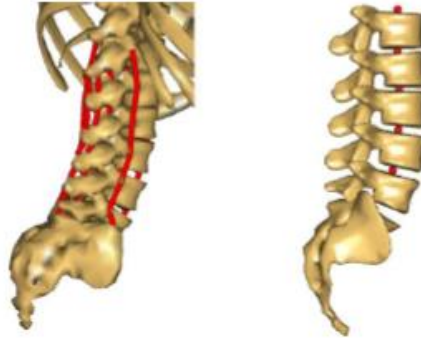
Figure 1.23 – Lumbar spine model developed by Galibarov and co-workers with the representation of the ligaments (left - red segments) and IVDs (right – red spherical joints) {Adapted from (32)}.

Han and co-workers published an article in 2012 that described a generic thoraco-lumbar spine model for the prediction of muscles forces. The bones of the model consisted of the skull, arms, legs, pelvis and spine. The cervical and thoracic spine was modeled as a single segment, while the lumbar spine as five rigid bodies. The model also simulated the muscles as single force components and the IVDs as rigid spherical joints with three rotational degrees of freedom. To validate the model they compare their results with data found in the literature (33).
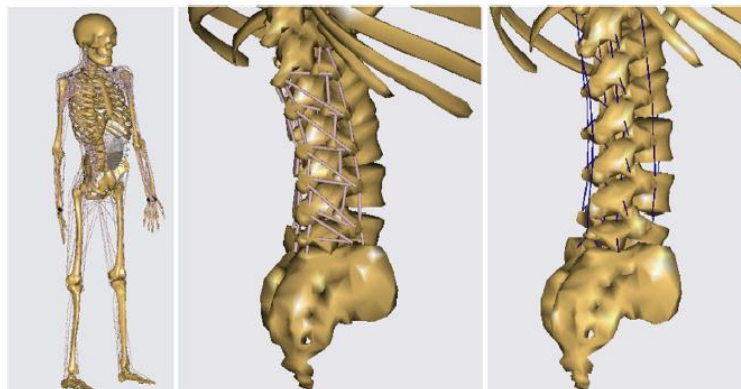
Figure 1.24 –Full body model representation (left) developed by Han and co-workers, lumbar muscle segments (middle) and lumbar ligaments (right) {Adapted from (33)}.

1.3. Objective

The aim of this work is the development of a three dimensional multibody system model of the lumbosacral spine using the Working Model ® software. The model must comprise all the vertebrae, ligaments, intervertebral discs and facet joints. The model can be used to study the

dynamic stability of the system, analyze the mechanical behavior and forces that the discs are subjected.

This work is part of the task T2.3B from the section WP2 of the European project "**NP Mimetic – Biomimetic Nano Fibre-Based Nucleus Pulposus Regeneration for the treatment of Degenerative Disc Disease**".

1.4. Structure of the thesis

The present thesis contains 6 chapters.

In the Chapter 1 it is possible to found the motivation of this work, a description of the literature review of the state-of-the-art of the multibody models of the spine and the main objective of this work.

The Chapter 2 focuses on the spine characterization, giving a brief anatomical description of the vertebra, facet joint, intervertebral disc and ligaments. In this chapter it also characterizes the spine movements and some pathologies related with the lumbar spine.

The main objective of the Chapter 3 is to summarize the concept of the multibody system dynamics and to describe the software used.

In the Chapter 4 describes the developed spine model, namely the lumbar vertebrae, the bushing elements, the movement equations, the ligaments and their mechanical properties and the facet joints. It is also possible to find the description about the model and the model's validation.

The Chapter 5 presents the movement analysis, namely about the forces and torques that each intervertebral disc is subjected during the simulated movements. It is also possible to find in this chapter the simulation and movement analysis of the fused spine.

The conclusion of this work and suggestions for future work are discussed in the Chapter 6.

The thesis end with a full list of references consulted during the work development.

Chapter 2 – Spine characterization

2.1   Anatomy of the Spine

The human spine, also called vertebral column, extends from the base of the skull, passes through the neck and ends at the pelvis. It protects the spinal cord and spinal nerves; supports the body's weight; provides an axis partially rigid and flexible for the body and a pivot for the head; plays an important role in posture and locomotion; serves as point of attachment for the ribs, pelvis and muscles of the back; and provides flexibility to the body that can flex up forwards, backwards and sideways and also rotate along its major axis.

The human spine is composed by thirty-three vertebrae distributed through five regions:

- Seven cervical vertebrae (C1-C7) in the cervical region which composes the axial skeleton of the neck, and it is responsible for supporting the head and allow motion;

- 12 thoracic vertebrae (T1-T12) in the thoracic region which suspends the ribs and support the respiratory cavity;

- 5 lumbar vertebrae (L1-L5) in the lumbar region which allows the mobility between the thoracic portion of the trunk and the pelvis;

- 5 fused sacral vertebrae (S1-S5) in the sacral region and connects the vertebral column to the bones of the lower limb girdle;

- 4 fused coccygeal vertebrae that support the pelvis floor (14).

The spine is not only composed by the vertebrae, but also by the intervertebral discs (that interconnects two adjacent vertebrae and allows relative motion between them), ligaments, muscles, articulation, and neural and vascular networks.

At the anterior and posterior view, the human spine does not present any curvature. But observed laterally (in the sagittal plane), the human spine presents several curves, which correspond to the different regions of the column (Figure 2.1). The cervical curvature is convex forward, the thoracic curvature is concave forward, the lumbar curvature is convex forward and the sacral or pelvic curvature is concave forward. The medical terms for the convex and concave curvature are lordosis and kyphosis, respectively. The reason why the spine presents natural

curvatures is due to the thickness of the intervertebral disc is not constant. At the cervical and lumbar region, the IVDs are thicker anteriorly than posteriorly. At the thoracic region, the opposite happens.
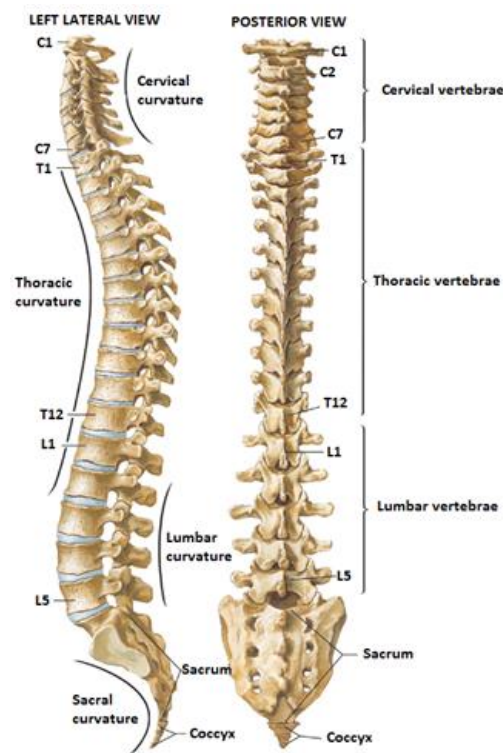
Figure 2.1 – General view of the human spine {Adapted from (34)}.

2.1.1. The vertebrae

The vertebrae structure differs depending in with region of the spine it is localized, but they all have some features similar. Every vertebra is composed by the vertebral body and its posterior elements, which include four articular processes, two transverse processes, one spinous process, two pedicle and two laminae (Figure 2.2). Between the superior and inferior surfaces there is an opening space called vertebral foramen where the spinal cord passes through (35).

The vertebral body is a disc-shaped portion that gives strength to the bone and it is essential to support the compressive forces of the spine. The load is transmitted from the superior end plate (top of the vertebral body) to the inferior end plate (bottom of the vertebral body) by two paths, the cortical shell (localized on the outside of the vertebrae) and the cancellous core (localized on the inside of the vertebrae) (5).

The two bones that extend laterally from each side of the vertebrae are called transverse processes. They serve for attachment of muscle and ligaments. The space between each

transverse process and the vertebrae body is called pedicle. The vertebra part that is palpable through the back is the spinous process. It is localized at the backward of the vertebrae and it is a projection that extends posteriorly. It is also a point of attachment for the muscle and ligaments. The part between the spinous process and the transverse process is called. There is four articular processes, two superior and two inferior, that are a union point of the pedicles and the lamina. The articular processes of two adjacent vertebrae limit the twisting of the vertebral column, because they touch and limit the movement. This contact area between two articular processes is called facet joint and it is covered by hyaline cartilage (35).

The size and mass of the vertebrae increase from the first cervical to the last lumbar vertebrae. This is a mechanical adaptation to the progressively increasing compression loads to which the vertebrae are subjected (5).
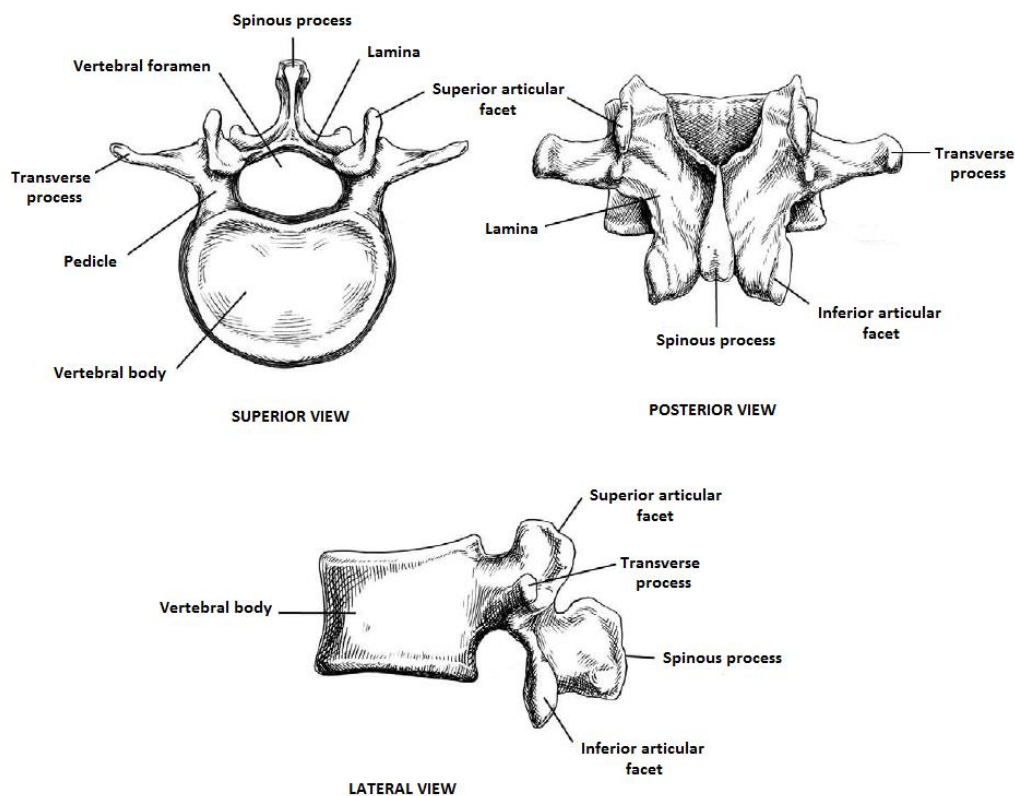
Figure 2.2 - Superior, posterior and lateral view of a typical vertebra {Adapted from (36)}.

2.1.1.1. Lumbar vertebrae

There are five vertebrae in the lumbar spine that can be easily identified by their heavy bodies and thick. Another specific feature of these vertebrae is that they are the largest vertebrae of all the spine and it is correlated to the forces loading that they are subjected and with the wide

range of movements, characteristic of this spine region. The lumbar vertebrae and IVDs resist about 80% of the compressive force acting on the spine (37).

The first four vertebrae are very similar. The vertebral bodies have large concave sides, the transverse processes are taper shape and they are directed laterally and backwards. The facet in the superior articular processes joint perfectly with the inferior facet of the vertebrae above, allowing a wide range of flexion, extension and lateral bending, but limits the axial rotation.

Comparatively with the others vertebrae, the fifth lumbar vertebra has shorter transverse processes and a less angular spinous process. Its inferior articular facets are widely separated facilitating a wide range of movement with the sacrum and prevent forward displacement of the vertebra (38).

2.1.1.2. Sacrum

The sacrum is a large, curved triangular bone formed by the fusion of five sacral vertebrae located at the base of the spine. It has the function of supporting the lumbar region and to transmit loads from the trunk to the pelvic girdle and into the lower limbs. The upper surface is similar to the upper surface of a typical vertebra. Below it is the coccyx, also called of tailbone, which is a small bone formed by the fusion of four vertebrae. The anterior and posterior sides of the sacrum sides of the sacrum contain four pairs of sacral foramina, through which nerves and blood vessels pass. The sacrum articulates with four bones: the last lumbar vertebra above (by the IVD and articulates processes), the coccyx (tailbone) below and the ilium portion of the hip bone on either side (38) (39).

2.1.2. Facet joints

A facet joint is formed by the articulation of the superior articular process of the vertebrae and the inferior articular process of the vertebra directly above it. It is a synovial joint covered by hyaline cartilage and a synovial membrane bridges the margins of the cartilage of the two facets in each joint. The hyaline cartilage diminishes the friction between the surfaces; and the synovial fluid lubricates it and diminishes surfaces wear. Surrounding the synovial membrane is a joint capsule that is reinforced by the ligamentum flavum and the posterior ligament in the lumbar region (39).

At the lumbar region, the shape of the articular facets is ovoid and they become oval from the first lumbar to the fifth lumbar. The joint is orientated perpendicularly to the transverse plane, increasing from the first lumbar to the fifth (like it is illustrated in Figure 2.3). The variations in shape and orientation of the lumbar facet joints limit the spine movement, specially the axial rotation.
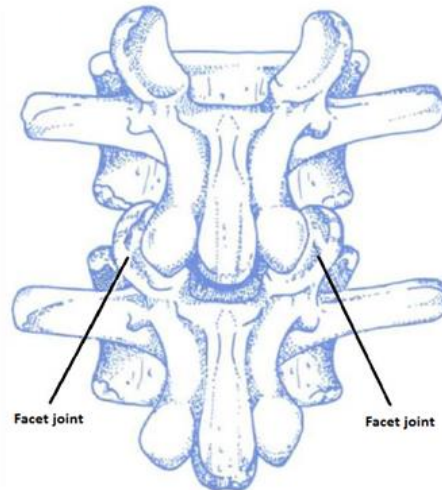
Figure 2.3 - Localization of the facet joint {Adapted from (39)}.

2.1.3. The intervertebral disc

The intervertebral disc is a disc shape interconnecting body between two adjacent vertebrae. In total, the human spine has twenty three intervertebral discs from C2 to S1. There is an element that separates the intervertebral disc from the vertebral body, a thin layer of hyaline cartilaginous end-plate. The intervertebral disc is a complex structure that is formed by two distinct parts: the nucleus pulposus and the annulus fibrosus.

2.1.3.1. Annulus fibrosus

The outer part of the disc is called annulus fibrosus and it forms a ring around the disc. The annulus is made up of a series of 15-20 concentric laminae of collagen fibres lying parallel within each ring and oriented at approximately 60◦ to the vertical axis, alternating to the left and right of it adjacent lamellae. The outermost layers are denser, resistant to tensile forces, they are attached to the endplates and the vertebral bodies and they are reinforced by the posterior and anterior ligaments. Between the lamellae lie elastin fibers that help the disc to return to its original position following bending, flexion or extension. The cells of the annulus are aligned

parallel to the collagen fibers, thin, elongated, and fibroblast like. The annular cells tend to become more oval as one moves inward toward the nucleus pulposus and the collagen fibers tend to become less dense and more loosely organized (40).

2.1.3.2. Nucleus pulposus

The inner part of the disc is the nucleus pulposus and it is a gelatinous core made up of collagen fibres (organized randomly) and elastin fibres (arranged radially) and booth fibres are embedded in a highly hydrated aggrecan containing gel. At the central region, the nucleus pulposus is more solidified composed of random type II collagen and irregularly shaped radially organized elastin (41).
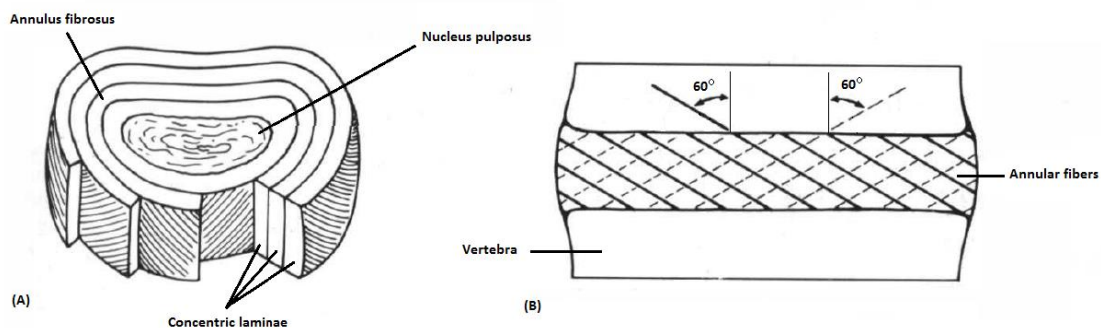
Figure 2.4 - Intervertebral disc. (A) Two parts of the intervertebral disc: Nucleus Pulposus and the concentric laminae of the annulus fibrosus. (B) Opposite fibres orientation at the annulus fibrosus of two adjacent laminae {Adapted from (40)}.

The lumbar intervertebral discs are the thickest of all the spine with, in average, 9mm and 40mm of diameter. Relatively to its nutrition, the IVDs are different from the other organs because they do not have blood supply. Its nutrition is made through the mechanical means of absorbing water into the disc when the individual is lying down, taking the weight off of the disc structure and the pressing out of the water out of the disc when upright walking, standing or sitting. Beside its function of linking the vertebrae, the IVD provides flexibility (bending, flexion and torsion), elasticity and compressibility to the spine. It also allows the spine to transmit loads (40).

2.1.4. The ligaments

The ligaments are a fibrous tissue that connects bones to each other and contributes to maintain structural stability. They also allow adequate physiologic motion, protecting the spine against excessive movements and they protect the neural structures. The ligament name depends of its localization (42). In each pair of vertebrae there are seven ligaments: the anterior

longitudinal ligament (ALL), the posterior longitudinal ligament (PLL), the interspinous ligament (ISL), the supraspinous ligament (SSL), the ligamentum flavum (LF), the intertransverse ligaments (TTL) and the capsular ligaments (CL) (Figure 2.5).
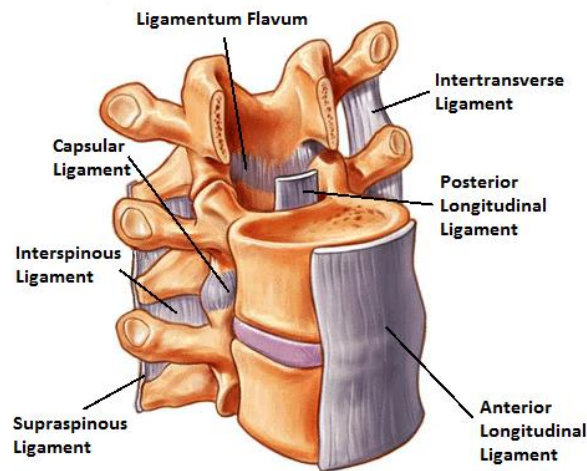
Figure 2.5 – Spine ligaments {Adapted from (25)}.

One important physical property of the ligament that helps to provide the physiologic function is the nonlinearity of the load-displacement curve (Figure 2.6). The curve can be divided into two ranges: physiologic and traumatic. The physiologic range includes two zones: neutral (small forces cause the displacement from the neutral position) and elastic (the displacement beyond the neutral zone until the physiologic limit). The traumatic range includes the plastic zone that is characterized by microtrauma with increasing load can lead to failure (5).
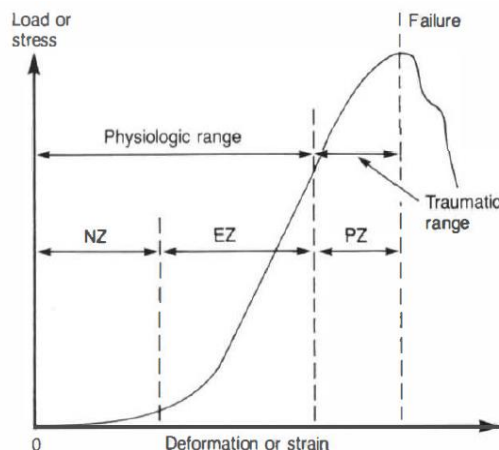
Figure 2.6 - Typical load-deformation curve of a ligament. NZ: Neutral Zone, EZ: Elastic Zone and PZ: Plastic Zone {Adapted from (5)}

The anterior and posterior longitudinal ligament, like the name indicates, lie on the anterior and posterior surfaces of the disc and are attached to the intervertebral disc and the vertebral bodies. They prevent the vertebrae separation, resisting the extension of the spine.

The supraspinous is the ligament that is closeness to skin, connecting the extremity of the spinous process of two adjacent vertebrae and its principal function is to prevent the separation of the spinous processes.

The interspinous process extends from the root to the apex of each spinous process. They limit the forward bending during the spinal movement.

The ligamentum flavum connects the laminae of two adjacent vertebrae. According with Dumas, G. *et al* (43), the ligamentum flavum is the most rigid ligament in traction and is the largest contributor to the whole ligament complex behavior. The function of this ligament is to prevent the separation of the laminae of adjacent vertebrae in flexion and extension movements.

The capsular ligaments are around the facet joint of the articular processes and they limit the axial rotation of the spine.

The intertransverse ligaments extend form the root to the apex of each transverse process connecting two adjacent vertebrae in this zone. This ligament has no mechanical significance in the lumbar zone because of it negligible cross-sectional size (5).

2.2 Spinal movements

The mobility of the spine results from the sum of individual movements of all the spine levels. The whole spine present four principal movements: extension and flexion, that corresponds to forward and backward bending in the sagittal plane), lateral bending in the coronal plane and axial rotation around the vertical axis (Figure 2.6). The degree of movement depends on the extensibility of the muscles and the ligaments and also the anatomy of the vertebrae (41).

The range of movement of the lumbar spine has been studied in a variety of ways, since cadavers and living subjects using clinical measurement or measurement from radiographs. The measurement obtained by the cadavers may not be corresponding movement on living subjects, because of the post-mortem changes, how they are kept up to measurements and because usually the back muscles are removed. On the other hand, with the cadavers the movement can be directly and precisely measured. The clinical measurement has the advantage that it measures the mobility of living subjects, but the measurements are limited (39).
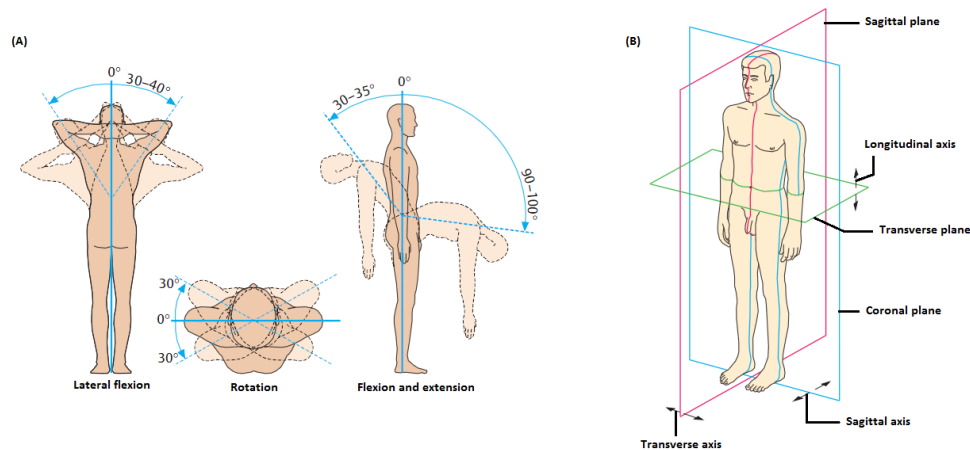
Figure 2.7 – Movement of the spine. (A) The four principal movement of the human spine: lateral flexion, rotation, flexion and extension. (B) Principal aces and planes of the human body {Adapted from (41)}.

Each lumbar level present six degree of freedom: three in translation (in each plane: sagittal, coronal and transverse – Figure 2.6 and three degree of freedom in rotation (around the three major axes). Besides these singular movements, the spine also presents coupled movement that result from two singular movements. The appendix A summarizes the limit and range of motion of each lumbar level, for the six singular movements, found in the literature.

2.3   Spinal disorders

Like any part of the body, all the spine elements also can suffer disorders due to traumatic injury, repetitive strain injury or due to age. The spine disorder represents over 50% of the causes for physical incapacity in labor age and they are one of the main causes for absence for work (44).

The common lumbar spine injuries are:

- Low back pain. This is an extremely common symptom in the general population. Usually it is caused by trauma, like lifting a heavy object. It also been associate with other spinal diseases like intervertebral disc degeneration.

- Disc herniation is the leakage of the nucleus pulposus through a hole of the annulus fibrosus wall. The hole of the wall can be caused by mechanical stress or aging.

- Intervertebral disc degeneration is characterized by the deterioration of the intervertebral disc and, consequently, it loose of function. This disease is related to mechanical stresses and also with aging. The disc degeneration can change the disc and, in the last stage, cause herniation or the collapsing of the two vertebrae.

- Spinal stenosis is a narrowing of the spinal canal due to the mechanical compression of the spinal root by the bones and soft tissues.

- Disc desiccation occurs when the water content of the nucleus pulposus is lost (14).

Chapter 3 – Multibody System

3.1. Multibody System Dynamics

The multibody systems are useful to study the biomechanics human motion and other biomechanical system's motion. A multibody system is composed by rigid and/or flexible bodies interconnected by kinematic joints that constraint their relative translational and rotational displacements, and actuated by external forces like the gravitational forces or others applied forces (Figure 3.1) (45).

A rigid body is when its deformations are very small and they will not affect the global motion. A flexible body is when the body shape can alter with internal dynamics. The kinematic joints link two bodies and constraint the relative motion between the bodies connected by the joint and they are responsible for determining the degree of freedom in the multibody system. The two typical kinematic joints are the revolute and the translational joint. The force elements represent the internal forces that are produced in the system and they are associated with the relative motion of the bodies. The forces applied can be the result of springs, dampers, actuators or external forces notes (45).
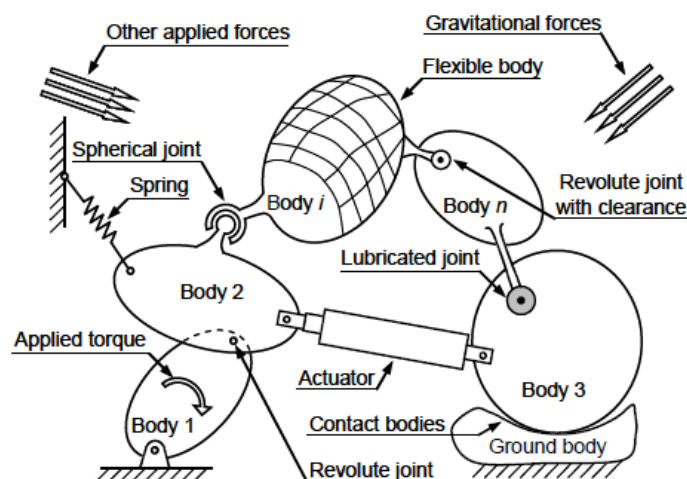
Figure 3.1 - Representation of a multibody system with the most significant components: bodies, joints and forces elements {Adapted from (45)}.

The multibody systems are used to study the system motion using two approaches: kinematic or dynamic. The kinematic approach aims to analyze the positions, velocities and acceleration of each

body at every instant of the analysis without considering the causes involved. On the other hand, with the dynamic approach it is possible to determine the motion of a system considering the produced forces. The dynamic approach can be analyzed by two ways: forward dynamic analysis, where the motion is determined as a result of the application of an external load; or inverse dynamic analysis where a particular movement is responsible for an internal force developed in each body (14).

3.2. Simulation software: Working Model

The software used to simulate the multibody system developed was the Working Model 4D ®. This is a simple user-friendly engineering simulation software that allows to construct complex systems.

With the software it is possible to define a set of rigid bodies (pre-defined in the program or import geometry from another software, e.g. AutoCAD) and constraints. It calculates the motion of interacting bodies using advanced numerical analysis techniques under a variety of constraints and forces. Besides the usual joints (rigid, revolute, spherical, slot, rods, ropes, separators, springs and dampers.) it is also possible to simulate multibody interactions such as collisions, gravity and external load conditions (forces, torques, actuators and motors). It is possible to create the joints exactly in the correct position by attaching a coordinate to a body and joint it to another coordinate to create the joint.

Each body has a set of physical properties that can be defined by the user, such as mass, coefficient of restitution, coefficient of friction, moments of inertia, positions and velocities. These bodies, constraints and external load properties can be defined by numerical or equation input using mathematical language.

The user can create a meter to plot the data that is generated during the simulation. It is possible to measure time, velocity, acceleration, positions, momentum, orientation, angular velocity angular acceleration, force, torque, friction and contact. These data can be exported to tab-delimited text files.

To simulate the system motion, the user can choose from Euler or Kutta-Merson integration techniques with fixed or variable time-stepping and they can also adjust error/accuracy levels and animation step (46).
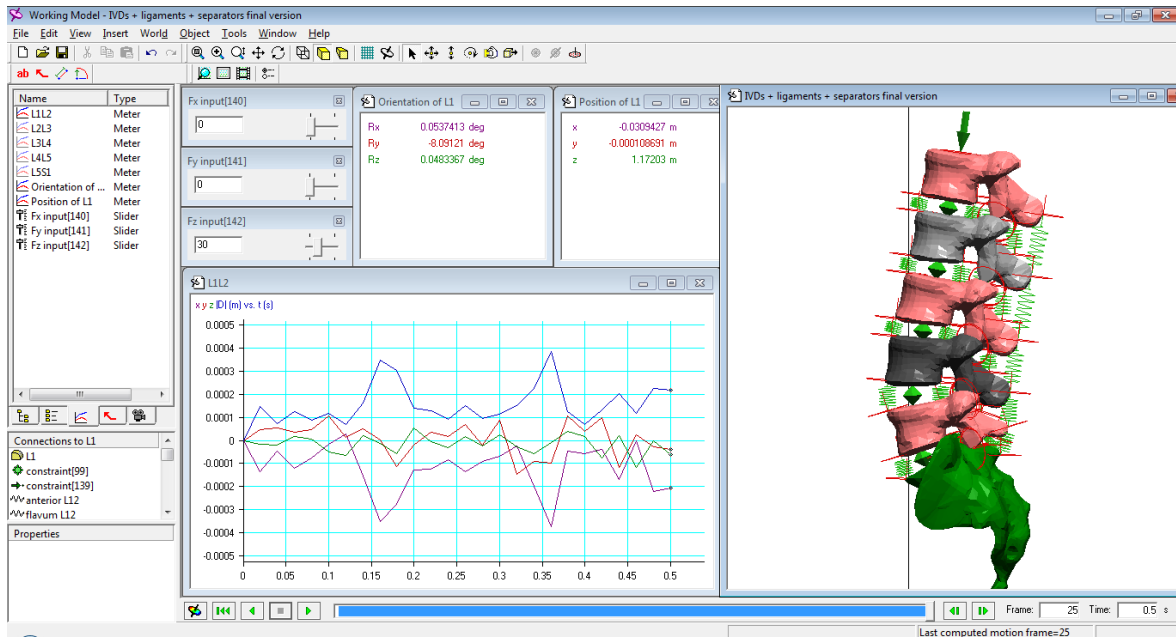
Figure 3.2 – Main window of Working Model 4D ®.

Chapter 4 – Biomechanical Multibody Spine Model

4.1. Description of the model

In this sub-chapter each element used for the multibody spine model is characterized based on literature. It is possible to find the vertebrae's world position and mass. For the intervertebral disc, their position and the movement equation used for each degree of freedom was described. For the ligaments it is possible to find their location and mechanical properties like the spring constant and pre-strain. Finally, both the location and contact of the facet joints was described.

4.1.1. Spatial reference system

The spatial reference system used in this work for the world position of the spine elements is illustrated at Figure 4.1.
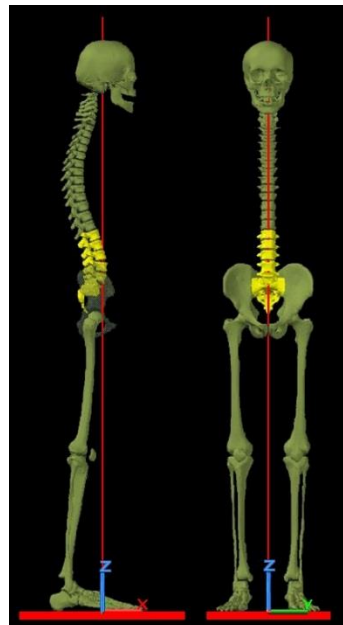
Figure 4.1 – Spatial reference system adopted.

4.1.2. Vertebrae

The vertebrae bodies used were collected from the internet, free data sharing. The vertebral bodies belong to a skeleton with 1.80m of height (Figure 4.1).

The localization and the angle of the sacrum was the same that the original. About the angles of the others vertebrae, the study was based into two radiographs and three Magnetic Resonance Imaging, to calculated the angles of the vertebrae with respect to the x axis line (horizontal). The position of the vertebrae was obtained from the thickness of the IVD (described later). The vertebrae mass used were the same that Keller et al (47) used in his work.

The angles, positions and masses of the lumbar vertebrae can be seen at Table 4.1.

Table 4.1 – The world position and orientation of the vertebrae used in MBS

Vertebra	Angle (∘)			Position (m)			Mass (kg)
	x	y	z	x	y	z	
L1	0	-8.5	0	-0.032	0	1.17307	0.17
L2	0	-6	0	-0.0315	0	1.13675	0.17
L3	0	-5	0	-0.025	0	1.09858	0.114
L4	0	-5	0	-0.018	0	1.06292	0.114
L5	0	15	0	-0.014	0	1.02479	0.114
S1	0	-1.7	0	-0.0333	0	0.98299	6

4.1.2. Intervertebral disc

To calculate the relative position of the vertebrae, corresponding to the IVD thickness, the same two radiographs and three MRI were used. A ratio was calculated between the vertebra height and the thickness of the IVD in the anterior and posterior; and then the mean. The next step was to calculate the thickness of the IVDs in the MBS developed based in the height of the vertebrae bodies. The thickness of the IVDs, the position and orientation of the Geometric Centre of the IVDs can be seen at Table 4.2 and the position of the vertebrae in the Working Model can be seen at Figure 4.2.

Table 4.2 – The world position, orientation and thickness of all the IVDs used in MBS

IVD	Angle (∘)			Position (m)			Thickness (m)
	x	y	z	x	y	z	
L1L2	0	-11	0	-0.02473	0	1.15675	0.007877
L2L3	0	-8	0	-0.01872	0	1.1197	0.00895
L3L4	0	-5	0	-0.01153	0	1.08235	0.010515
L4L5	0	1	0	-0.00528	0	1.04368	0.011588
L5S1	0	22	0	-0.00875	0	1.006001	0.00719

Figure 4.2 – Final position of the vertebrae in the Working Model

The intervertebral discs were modeled as 6 degree of freedom bushing elements.

4.1.2.1. FEM

The FEM analysis from the project group of this work simulated two vertebrae linked with an intervertebral disc. The points for the movement equation were obtained from a motion analysis. For the three rotations, the torque was applied on the upper vertebra and, consequently, the vertebra motion was determined. The torque values used for the three translations were: -10, -7.5, -5, -2.5, 2.5, 5, 7.5 and 10 Nm. To obtain the points for the translation movement the methodology was reversed. The vertebrae motion was imposed, then the software determined the force value that originated the vertebrae's motion. The motion values used for the flexion/extension and lateral bending were: 0.0004m until -0.0004m and for the compression/traction were: -0.0013m until 0.002m.

4.1.2.2. Motion equations

The bushing elements depend of their spring and damper constant; and to characterize the spring constant, it was used the data from the FEM analysis. To determine the spring constant's equation, 3 steps were followed. First, the spring constant of each point using the following equation: $k = \frac{Force}{Displacement}$ was calculated. Secondly, a graph of spring constant in function of motion was created and the equation was determined. Finally, the equations were adjusted until the vertebrae motion was in concordance with the FEM analysis. The Table 4.3 summarizes the spring constant's equation used for each simulated movement.

Table 4.3 – The spring equation used for each simulated movement

Movement	Spring equation
Translation in x	$1 \times 10^{10}x^2 - 2 \times 10^6 x + 173769$
Translation in y	$1 \times 10^{10}x^2 + 3500x + 156521$
Translation in z	$8 \times 10^{10} - 3 \times 10^8 x + 1.5 \times 10^6$
Rotation in x $]-\infty, 0]$	$-0.0131x^2 - 0.0016x + 125$
Rotation in x $]0, +\infty]$	$0.0707x^4 - 0.9722x^3 + 4.7591x^2 - 9.5936x + 120$
Rotation in y $]-\infty, 0]$	$-0.0006x^2 + 0.0366x + 71$
Rotation in y $]0, +\infty]$	$0.0475x^4 - 0.6532x^3 + 3.2132x^2 - 6.4813x + 90$
Rotation in z $]-\infty, 0]$	$-0.1431x^2 + 7e^{-15}x + 300$
Rotation in z $]0, +\infty]$	$0.1694x^4 - 2.3287x^3 + 11.289x^2 - 22.646x + 300$

The damper coefficient used was 100 Kg/s and 0.01 N.m.s/deg for translation and rotation, respectively.

4.1.2.3. Comparison between FEM and WM

In the Figure 4.3, a comparison between the vertebra's motion in function of the force from the FEM analysis and the WM simulation was made.

In general, the vertebrae's motion in the WM was very similar with the vertebra's motion from the FEM, especially during the translation in y and rotation in z. During the translation in z, rotation in x and y, the curves are mostly coincident having a slight differences at the extremities. The curve from comparison during the translation in x is the curve that presents higher differences between the two analyses, however those differences are not significant.
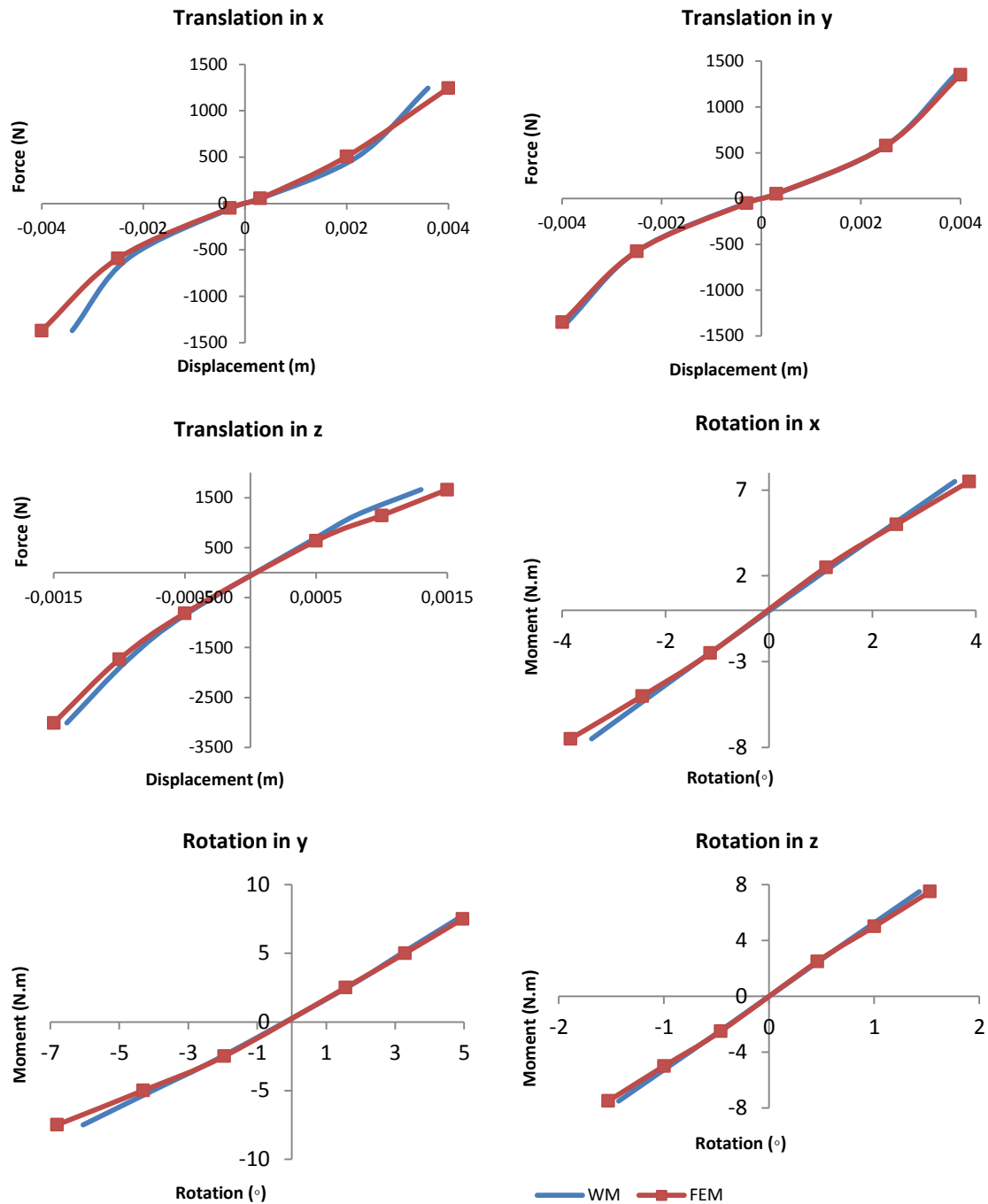
Figure 4.3 - Comparison between the displacement in function of the force from the WM and the FEM analysis for all the simulated movements.

4.1.3. Ligaments

To determine the position of the ligaments, this study was based in the work of Monteiro, N. (8). Then, the ligaments' positions were adjusted to the geometry of each vertebra. The coordinate's local position, which defines the ligament on each body, can be seen at Table 4.4 and 4.5.

Table 4.4 – The local positions of the coordinates which defines the ligaments

Vertebra	Anterior			Posterior			Flavum		
	x	y	z	x	y	z	x	y	z
L1	0.022	0	-0.012	-0.011	0	-0.0119	-0.02087	0	-0.008
L2	0.027	0	0.015	-0.006	0	0.012	-0.0172	0	0.001
	0.028	0	-0.012	-0.004	0	-0.0119	-0.0172	0	-0.012
L3	0.026	0	0.016	-0.0062	0	0.0119	-0.0165	0	0.001
	0.029	0	-0.012	-0.0037	0	-0.0115	-0.0165	0	-0.012
L4	0.027	0	0.014	-0.00515	0	0.0127	-0.0166	0	0.001
	0.027	0	-0.013	-0.005	0	-0.0111	-0.0166	0	-0.008
L5	0.022	0	0.016	-0.00969	0	0.01061	-0.0197	0	0.0008
	0.022	0	-0.012	-0.00575	0	-0.0113	-0.0197	0	-0.008
S1	0.035	0	0.009	0.011575	0	0.025219	-0.00089	0	0.030734

Table 4.5 - The local positions of the coordinates which defines the ligaments (continued)

Vertebra	Interspinous			Supraspinous			Interspinous and supraspinous		
	x	y	z	x	y	z	x	y	z
L1	-0.035	0	-0.02	-0.052	0	-0.01338	-0.07169	0	1.14546
L2	-0.0341	0	-0.00403	-0.0455	0	-0.016	-0.07185	0	1.1246
	-0.03	0	-0.024				-0.06860	0	1.10731
L3	-0.03403	0	-0.0055	-0.045	0	-0.016	-0.06541	0	1.08608
	-0.02781	0	-0.024				-0.05972	0	1.0687
L4	-0.03342	0	-0.00219	-0.047	0	-0.013	-0.05959	0	1.05416
	-0.03	0	-0.022				-0.05556	0	1.03632
L5	-0.03147	0	-0.00054	-0.044	0	-0.014	-0.05863	0	1.02549
	-0.034	0	-0.017				-0.05648	0	1.01699
S1	-0.01287	0	0.031	-0.021	0	0.025	-0.05316	0	1.01179

4.1.3.1. Mechanical properties

The ligaments were modeled as spring elements and to define the spring constant the work of Chazal *et al* (48) was used. The force-deformation curves of the lumbar ligaments (Figure 4.4) are nonlinear. They have an initial phase in which a small force produces large deformation and a latter phase where the ligament is stiffer.
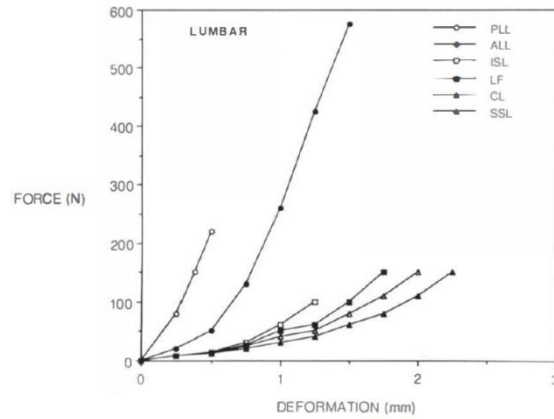
Figure 4.4 - Force-deformation curves of lumbar ligaments. PLL=posterior longitudinal ligament; ALL=anterior longitudinal ligament; ISL=interspinous ligament; LF=ligamentum flavum; CL=capsular ligament; SSL=supraspinous ligament {Adapted from (5)}.

In the study of (48), 43 human spinal ligaments from fresh cadavers and living subjects and the tensile tests were performed with an original testing machine. To choose the curved for each ligament, it was chosen the lumbar spinal, dead subjects and with the age similar (around 63 years-old). For the lumbar spine, Chazal tested the supra and interspinous ligament together. The Table 4.6 and 4.7 show the key points for the force-deformation curve and the corresponding spring constant to each segment.

Table 4.6 - Some points of the force-deformation curve of each lumbar ligament and the spring constant (k) associated to each segment using the curve of (48)

ALL			PLL		
Force (N)	Displacement (m)	k (N/m)	Force (N)	Displacement (m)	k (N/m)
0	0	800	0	0	7500
8.8	0.001	9000	33.8	0.0005	5500
60	0.002	60000	60	0.0009	50000
450	0.0044	60000	330	0.0036	52000
520	0.0065		360	0.0042	

Table 4.7 - Some points of the force-deformation curve of each lumbar ligament and the spring constant (k) associated to each segment using the curve of (48) (continued)

SSL ISL			LF		
Force (N)	Displacement (m)	k (N/m)	Force (N)	Displacement (m)	k (N/m)
0	0	26300	0	0	6000
26.3	0.001	40000	36.1	0.001	4000
60	0.0016	85000	75	0.0016	45000
270	0.0034	72000	315	0.0038	44000
300	0.0044		340	0.0048	

The comparison between the force-deformation curves from (48) and from the Working Model can be seen at Figure 4.5. The curves of force-displacement are very similar, having a maximum percentage of discrepancy of 2.52, 0.5, 0.11 and 1.7 for the posterior longitudinal ligament, anterior longitudinal ligament, interspinous and supraspinous ligament and ligamentum flavum, respectively.
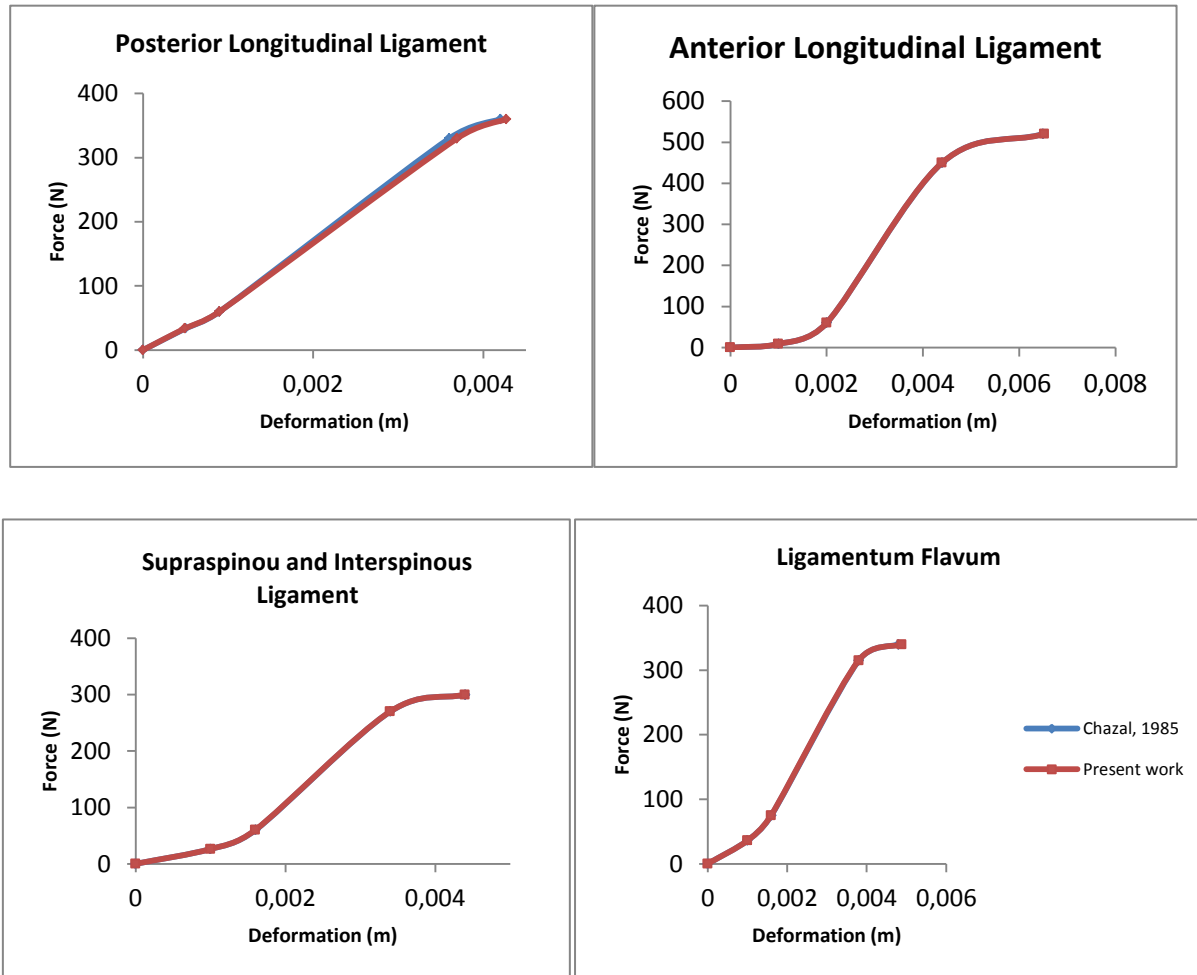
Figure 4.5 - Comparison between the force-displacement curves of the ligaments from (48) and from the Working Model.

4.1.3.2. Pre-strain

Another important characteristic of the ligaments it's their pre-strain. During the mechanical tests, the authors reported that the ligament's length decreased after removing them from their natural location. To quantify the pre-strain, a measurement of the ligament's length was made before and after the ligament's removal from the motion segment. In the literature it was possible to find some percentage of pre-strain (Table 4.8).

Table 4.8 – Pre-strains found in the literature for the ligaments

Spine region	Pre-strain (%)					Reference
	ALL	SSL	ISL	PLL	LF	
T12-S1	2.0 +- 4.4 n=7	-6.0 +- 12.7 n=9	4.3 +- 6.7 n=9			(49)
Lumbar	3.4 +- 0.4 n=4			10.5 +- 0.6 n=4	17 n=1	(50)
Not mencioned	7.98 +- 2.28 n=28			9.88 +- 2.5 n=28		(51)
L3-L4					10.59 +- 5.56 n=10	(52)
Not mencioned		-0.85				

From the published results, some ligaments present more than one pre-strain, and to diminish the error it was choose the pre-strain of the most representative sample available. In the human body, the ligaments only work on traction by constraining the vertebrae's motion. On compression the ligament's work is null. Since the SSL and ISL present negative pre-strain, it was assumed that the ligament's force-deformation curve only begins when the ligament's deformation is superior to the natural length. Before the ligament's natural length, the spring constant is equal to its first segment. An example of the spring equation for the supraspinous and interspinous ligament is shown at Figure 4.6.
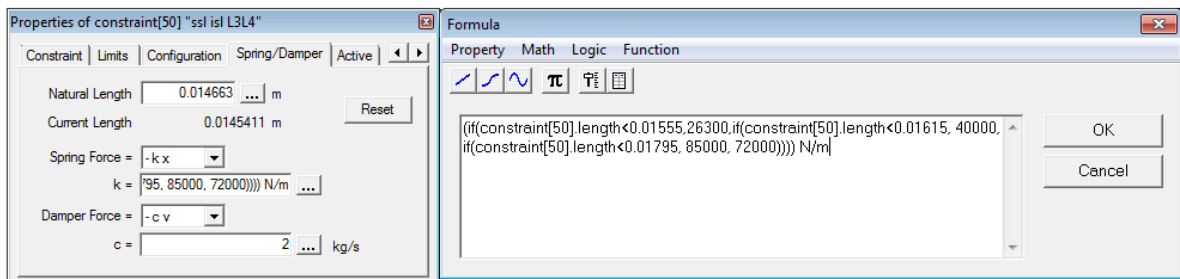
Figure 4.6 – Example of the spring constant formulation for the supraspinous and interspinous ligament.

4.1.4. Facet joints

To determine the position and the orientation of the facet, it was used the data found in the literature. About the position, it was used a ratio height/length of the vertebrae based on Figure 4.7(A), and then the position of the facets of the multibody was calculated. About the orientation, it was used the angles described in White *et al* (5) and they can be seen at Figure 4.7(B).
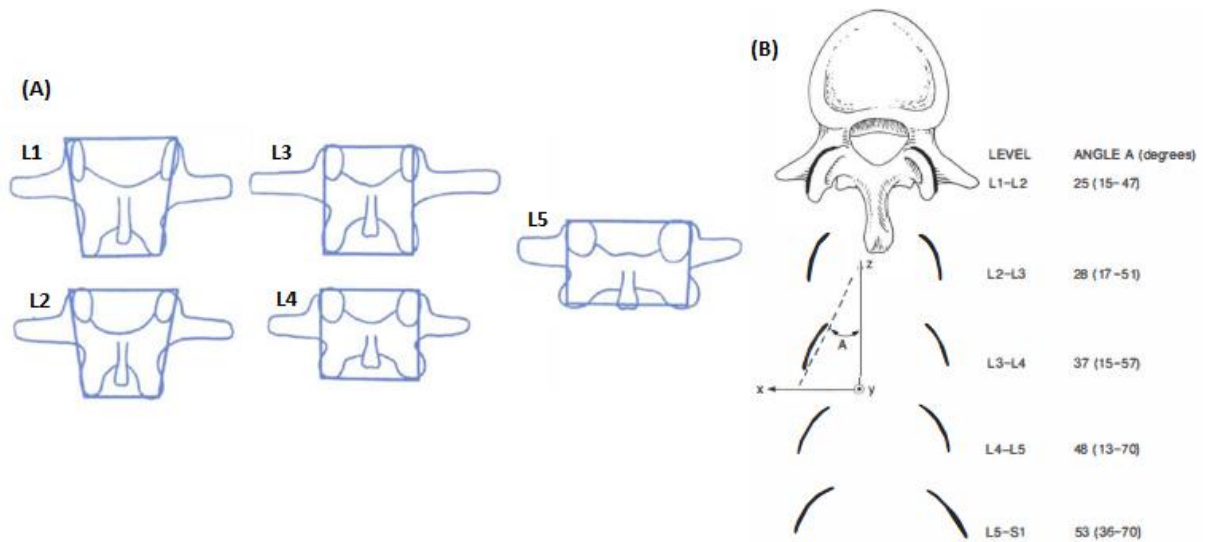
Figure 4.7 – Facet joints. (A) Localization of the facet joints of the five lumbar vertebrae. (B) Shape and inclination of the facets of the lumbar spine in the transverse plane along the levels {Adapted from (39) and (5)}.

According with Weishaupt *et al* (53), the normal joint space is 2-4mm, so it was decided to use 3 mm for all the facet joints. The position and orientation of the facet joints used in the multibody are described at Table 4.9.

Table 4.9 - The world position and orientation of the facet joints used in MBS

	Position (m)			Orientation (°)		
	x	y	z	rx	ry	rz
L1	-0.0536998	0.01	1.149	71	-25	161
	-0.0536998	-0.01	1.149	-71	-25	161
L2	-0.0536998	0.013	1.149	71	-25	161
	-0.0536998	-0.013	1.149	-71	-25	161
	-0.0487356	0.01031	1.11059	71	-28	161
	-0.0487356	-0.01031	1.11059	-71	-28	161
L3	-0.0487356	0.01331	1.11059	71	-28	161
	-0.0620456	0.01331	1.11059	-71	-28	161
	-0.0413255	0.01216	1.07537	71	-37	161
	-0.0413255	-0.01216	1.07537	-71	-37	161
L4	-0.0413255	0.01516	1.07537	71	-37	161
	-0.0413255	-0.01516	1.07537	-71	-37	161
	-0.0360881	0.01586	1.04141	71	-48	161
	-0.0360881	-0.01586	1.04141	-71	-48	161
L5	-0.0360881	0.01886	1.04141	71	-48	161
	-0.0360881	-0.01886	1.04141	-71	-48	161
	-0.0391431	0.02067	1.01164	71	-53	161
	-0.0391431	-0.02067	1.01164	-71	-53	161
S1	-0.0391431	0.02367	1.01164	71	-53	161

The facet joints were modeled as separators between the two coordinates that locates the contact area of the facet joints in each vertebra. A separator applies forces at its endpoints so that they do not become closer than a specified distance – separator length. Since the facet joints aims to limit the movement, the separator length was defined as null, so that the contact area of each facet joint could touch but not penetrate.
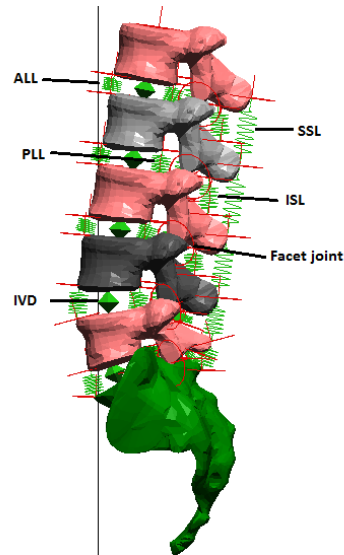
Figure 4.8 - Final MBS of the lumbar spine.

4.2. Validation of the model

This sub-chapter describes the stages for the model validation. Part of the validation used the spinal motion measured in cadavers when subjected to forces and torques. The second part used the data from OrthoLoad.

4.2.1 Data from the literature

The work of Panjabi *et al* (54) presents a complete three-dimensional motion of each lumbar intervertebral level. They used nine whole fresh-frozen human cadaveric lumbar-spine specimens. They apply pure torques of flexion-extension, bilateral axial torque and bilateral lateral bending and the motions were determined with the use of stereophotogrammetry.

The work of Guan *et al* (56) tests the hypothesis that the human lumbosacral joint behaves differently from L1-S1 joints. The musculature was removed of ten cadavers and then they were subjected to pure torque flexion and extension and left-right lateral bending. The motion was measured with a four-camera optoelectronic system.

Both work's procedure was simulated in the Working Model in order to validate the multibody. The comparison between the published results and the multibody motion, during the flexion-extension, can be seen at Figure 4.9.
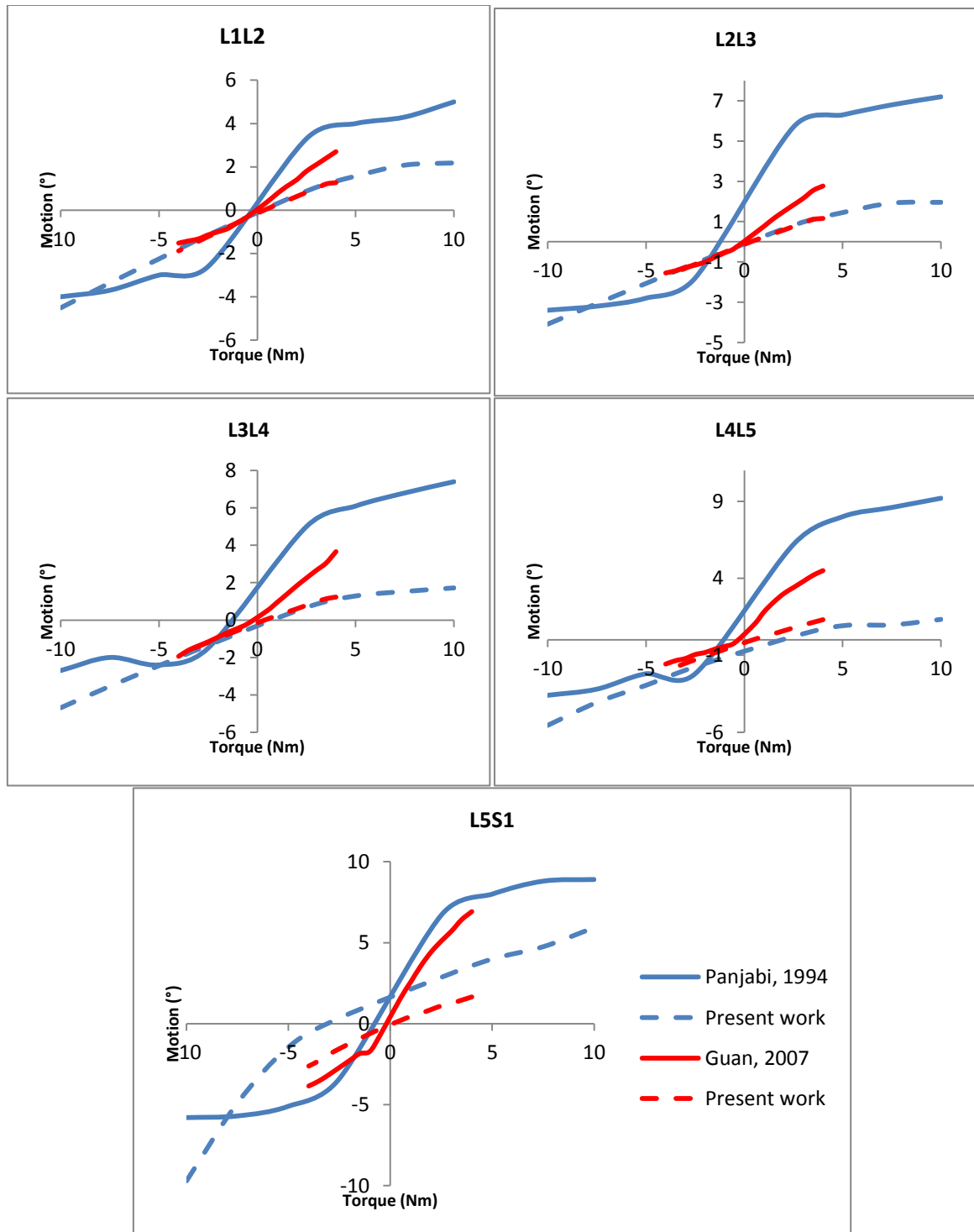
Figure 4.9 - Comparison of the MBS motion measured with Working Model and the published results during the flexion-extension of the spine.

Interpreting the graphs of Figure 4.9, the first aspect that is highlighted is the fact that the MBS is more rigid, especially in flexion, comparing with the data from the literature. However, the MBS motion comparing with the results of Guan *et al* are more similar, especially during the extension, except for the level L5S1. Interpreting the curve from the MBS, it can be seen that the rotation during the extension is higher than the rotation during the flexion. This is contrary to the physiologic motion, because the spine is more flexible in flexion than in extension. This excessive rigidity of the MBS during flexion can be a consequence of the excessive rigidity of the ligaments. During the flexion there are three ligaments that mainly influence the movement: supraspinous, interspinous and ligamentum flavum. On the other hand, during the extension, only two constraints the movement: anterior and posterior longitudinal ligament. Besides the excessive rigidity of the ligaments, it can also be due to the high rigidity of the IVD from the FEM analysis. The MBS curves are more linear, but they behave like the curve from the literature, responding with an increase of motion when the torque is higher and vice-versa. From the published data, the motion between the fourth and fifth lumbar vertebrae and the fifth lumbar and first sacral vertebrae were significantly greater than the motion of the others lumbar levels. With the MBS similar happens during the extension.

According to (54), besides the rotation they also measured translation in the sagittal plane in all the levels. But in the MBS, the translations are very small in order of microns. Maybe this is due to the rigidity of the MBS.

The Figure 4.10 compares the lateral bending from the literature and the motion of the MBS measured in the WM. The motion's curves from the literature behave the same way and the same happens with the motion's curves from the MBS motion. The MBS curves are more linear whereas the curves from the literature seem to have two phases: nonlinear and linear. The motion during the left (negative) torque is lower than the right torque in all curves. This is normal, because the human body is not symmetric. The authors report that there is a greatest motion between the second and third lumbar vertebrae, comparing with the others levels, and the same happens with the MBS although the difference is not so great. Comparing the rotation, the MBS seems to be more rigid, but the differences between the curves decrease with the torque increasing (for both sides).
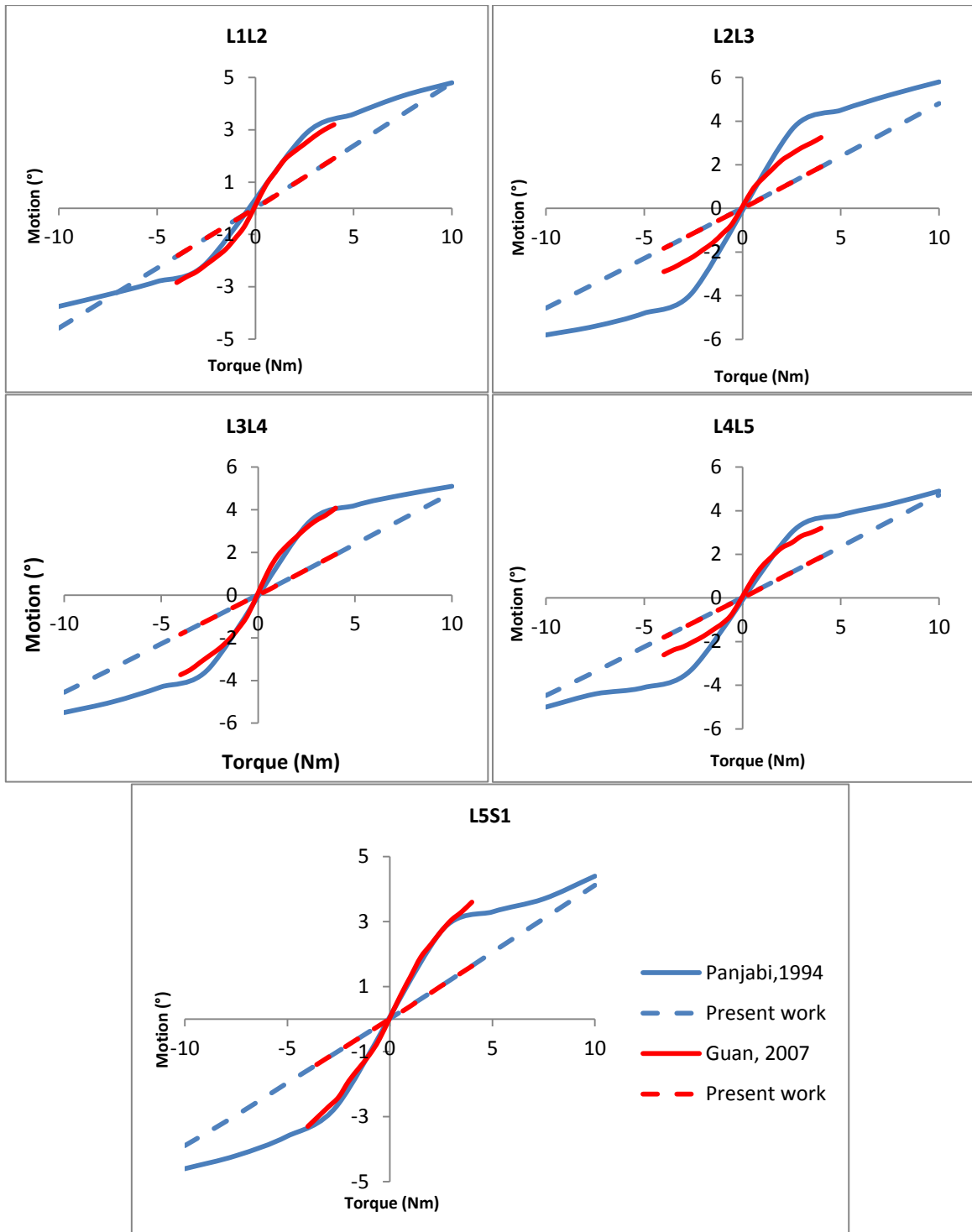
Figure 4.10 - Comparison of the MBS motion measured with Working Model and the published results during the lateral bending of the spine.

Like the flexion-extension, Panjabi *et* al (54) reported coupled rotations associated to the lateral bending: flexion-extension rotation and axial rotation. The Figure 4.11 compares the coupled motion during the lateral bending. During this movement, the coupled rotations found in the literature are

very different from the MBS. The data from the paper are very irregular whereas the coupled rotations from the MBS are more constant and similar between them.
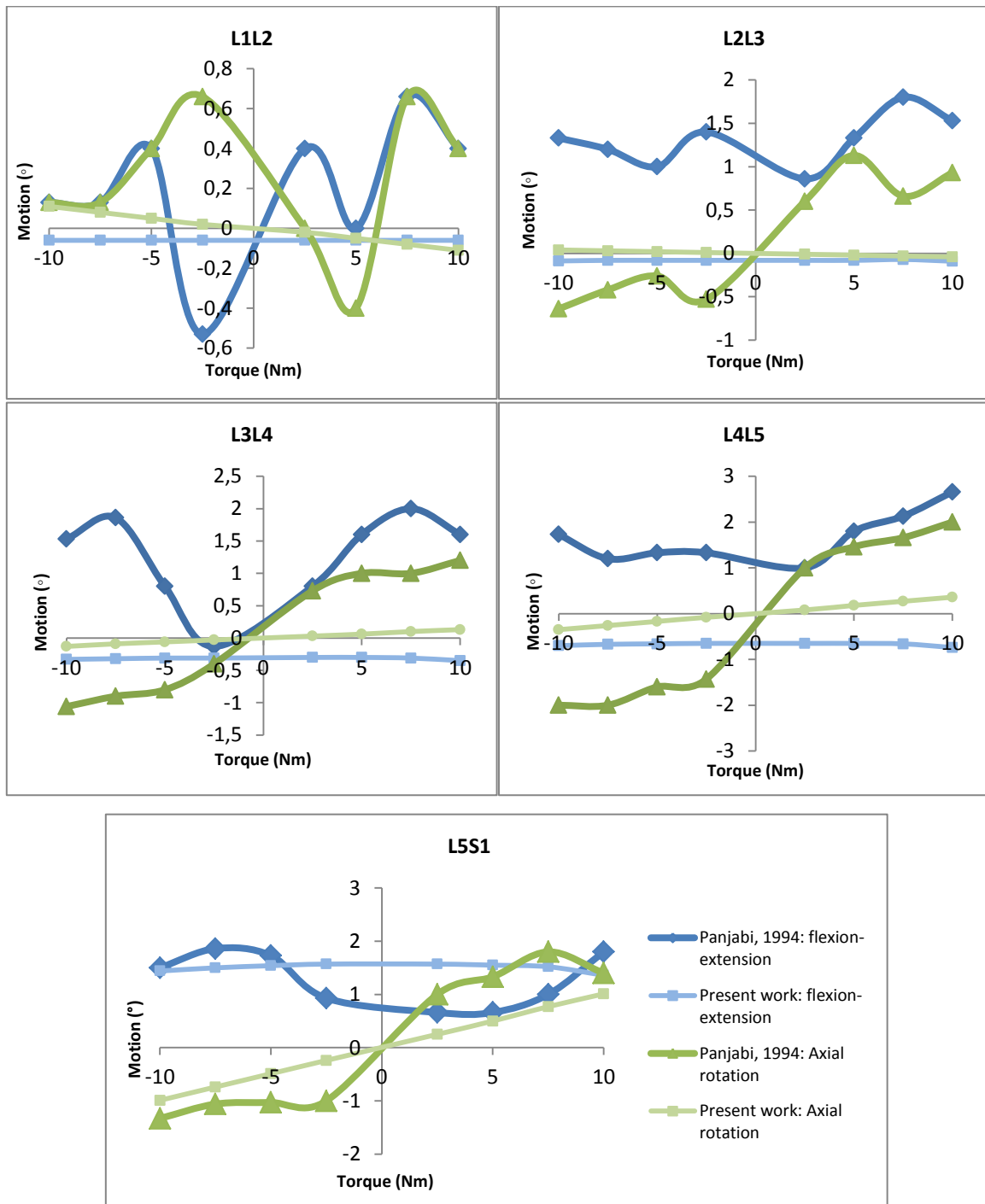
Figure 4.11 - Comparison of the MBS coupled rotation and the coupled rotation measured by Panjabi and co-workers during the lateral bending movement.

The Figure 4.12 compares the MBS motion and the motion from (54) during the axial rotation.
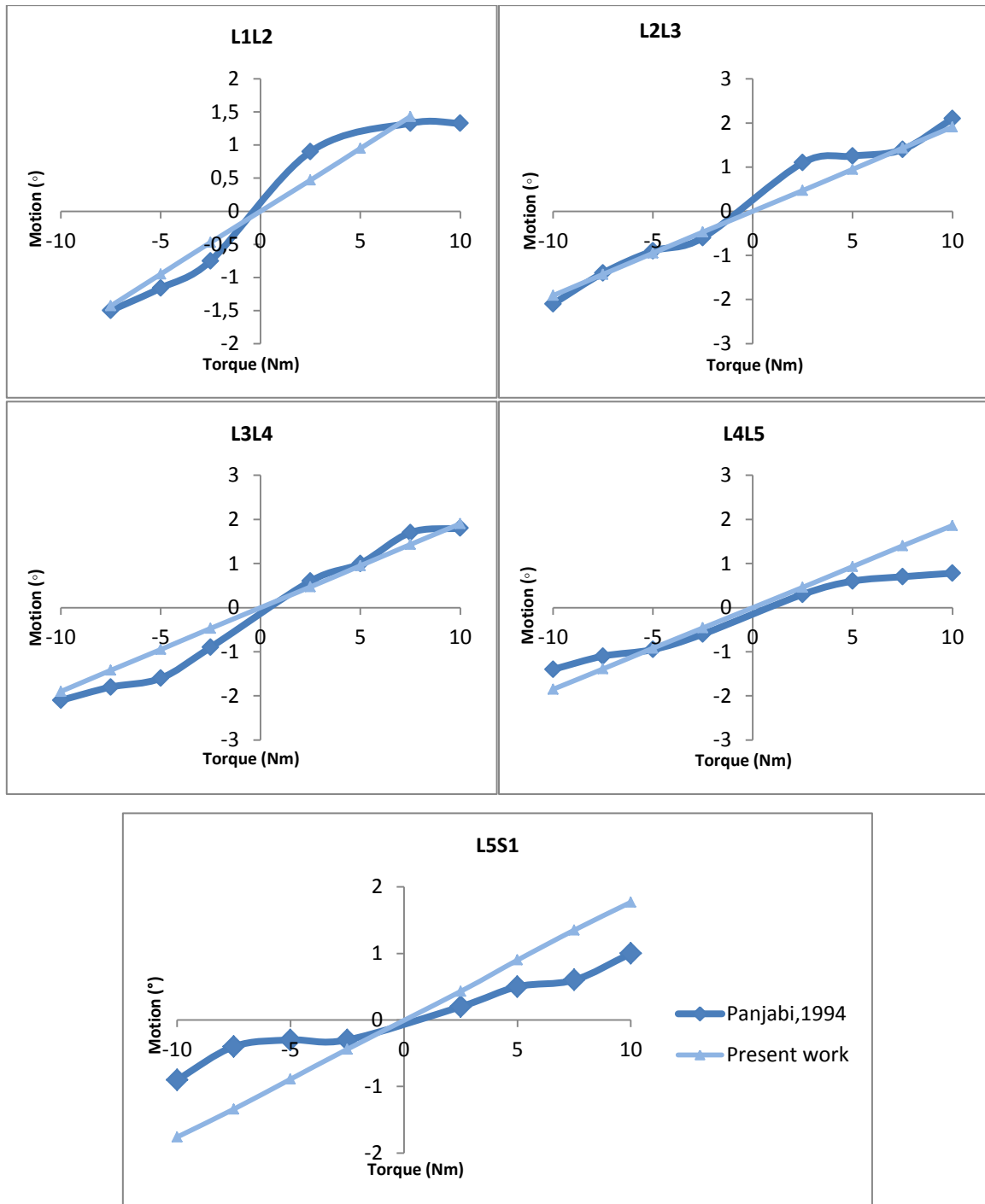
Figure 4.12 - Comparison of the MBS motion measured with Working Model and the motion measured by Panjabi and co-workers during the axial rotation of the spine.

In general, the behavior of both curves is very similar, having some coincident points, especially from L1L2 until L4L5. In his work, Panjabi and his co-workers mentioned that there is a significantly higher motion between the second and third lumbar vertebrae than between the fourth and fifth lumbar vertebrae, but in the MBS motion that does not occur. The axial rotation decrease from the L1 to S1 progressively. Unlike what happen during flexion-extension, during the axial rotation the

MBS, in some levels, presents higher flexibility. This can be due to the fact that the capsular ligament was not implemented, just the facet joint. The capsular ligament will act like a cushion amortizing the contact between the facet joints, like the cartilage that covers the joint. The other function of the capsular ligament is to avoid the excessive distance between the facets joint. From the curve force-deformation of White *et al* (5) it could be characterized the spring constant of the ligament, but an obstacle to the simulation of the ligament is that it was not found the pre-strain that the ligament is subjected and the work of Chazal *et al* (48) did not study the capsular ligament. In the data from the paper, it is notable that the axial rotation is not symmetric in both sides, being greater with right (negative) torque than with left torque. In the MBS this asymmetry does not occur.

According to the authors, the rotation axial has coupled flexion-extension rotations and lateral bending rotation in both sides. The Figure 4.13 compares the coupled motion during the axial rotation. In some levels the coupled rotation of the MBS are very similar with the rotation measured by (54), like L5S1.
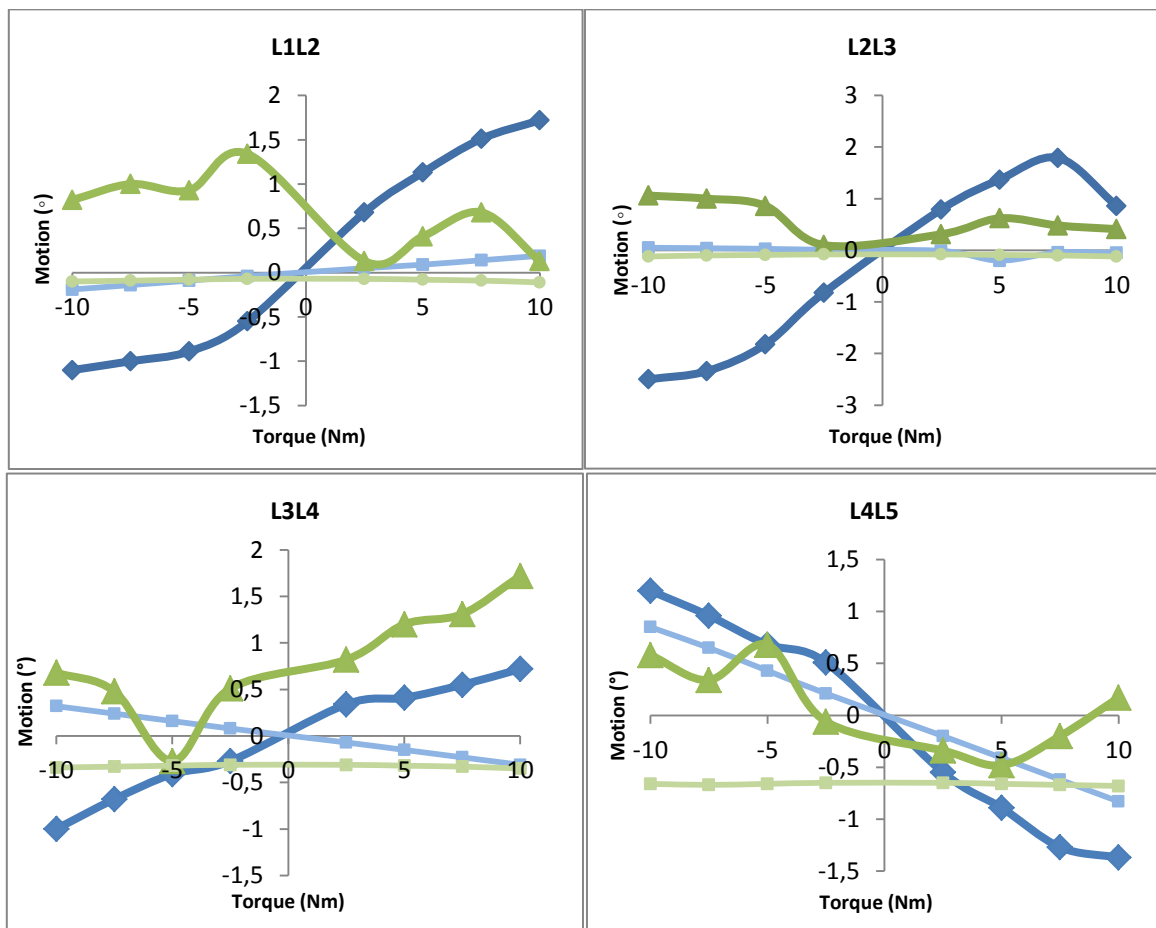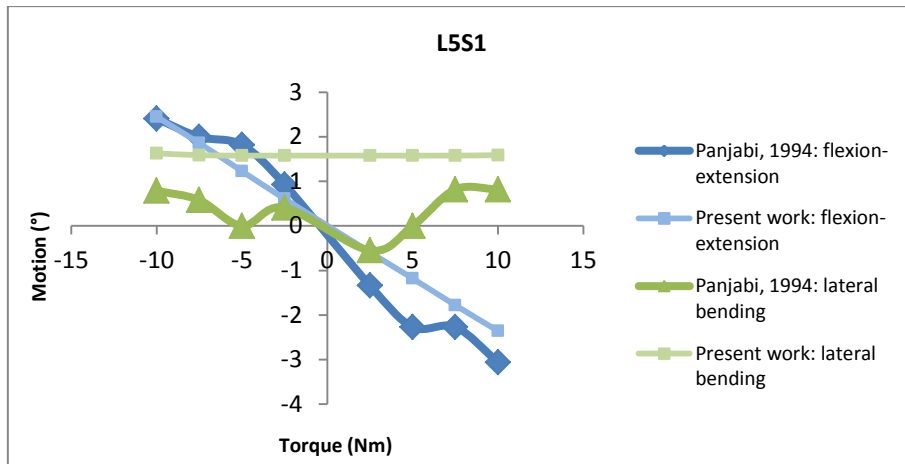
Figure 4.13 - Comparison of the MBS coupled rotation and the coupled rotation measured by Panjabi and co-orkers during the axial rotation.

The work of McGlashen *et al* (55) studied the L5S1 spine motion of nine fresh adult cadavers with the ligaments and joints intact. The work result of a three dimensional load displacement behavior of the lumbosacral joint. They applied forces to the geometric center of the inferior L5 endplate through a system of cables and pneumatic cylinders; S1 was rigidly fixed to the testing apparatus with the inferior endplate of L5 mounted horizontally. The forces applied were 160N for the lateral, anterior and posterior shear, 320N in compression and test torques of 15.7 Nm in flexion, extension, lateral bending and torsion.

Once again the procedure used in the work of McGlashen and his co-workers was reproduced with the MBS in WM to compare the motion. The Table 4.10 summarizes the lumbosacral joint motion form the paper and the MBS during the tested movements.

Table 4.10 – Motion of the lumbosacral joint form the paper and WM during the movement tested

Movement	Load	Motion (∘ or mm) from paper	Motion (∘ or mm) from WM
Compression	320 N	0.32	0.2
Lateral Shear	160 N	1.65	1.6
Anterior Shear	160 N	2.05	1.4
Posterior Shear	160 N	2.21	1.6
Torsion	15.7 Nm	3.38	2.93
Flexion	15.7 Nm	7.19	3.87
Extension	15.7 Nm	5.16	10.35
Lateral Bending	15.7 Nm	4.38	7.5

Comparing the results from the Table 4.10, some MBS motions are very similar with the motion measured by (55) like the lateral shear, compression and torsion. The lateral shear has the lowest

motion comparing with the others shears, in the paper, but the opposite happen in the MBS. Comparing the posterior and anterior shears, once again, the MBS present a higher rigidity. During the flexion-extension, the mobility of the MBS is completely opposite to the motion from the measured values, presenting higher mobility during the extension than during the flexion.. During the lateral bending, the MBS present higher motion (almost the double).

4.2.2 OrthoLoad

OrthoLoad is a public database containing the loads acting in orthopaedic implants. They measured *in vivo* forces and torque on several implant, using instrumented implants with telemetric data transmission. The implant that was used was the vertebral body replacement (Figure 4.14). All data is presented as videos, containing the time-dependent forces and torques, force vectors, video images of the patients and numerical data. From their database it is possible to select an implant, an activity, a patient and one or several trials. The videos can be analyzed in more detail by displaying single video frames.

Figure 4.14 – Vertebral body replacement of OrthoLoad {Adapted from (57)}.

To validate the model with the correct equation of the spring constant, four basic movements were selected: flexion at 90°, simple flexion, extension and lateral bending.

The videos were analyzed with the Physmo software. The software is a video motion analyzer and allows following the movement of a point (or several) during the video. The first step was to localize the coordinate system. (Figure 4.15(A)) The following step was to place the points in the respective place (Figure 4.15(B)). In this case the points were put in the pelvis zone and close to the L1 vertebra. To help with the pointing task, the software has the choice to choose the option 'show edges' that transform the image so that is easier to place the point without make large error (Figure 4.16). After that, the video was played and stopped when the person reaches the position in study.

One more time the points were placed in the respective place, and at the left side of the window (Figure 4.15(C)), the software calculates the exact position of each point in the two positions.
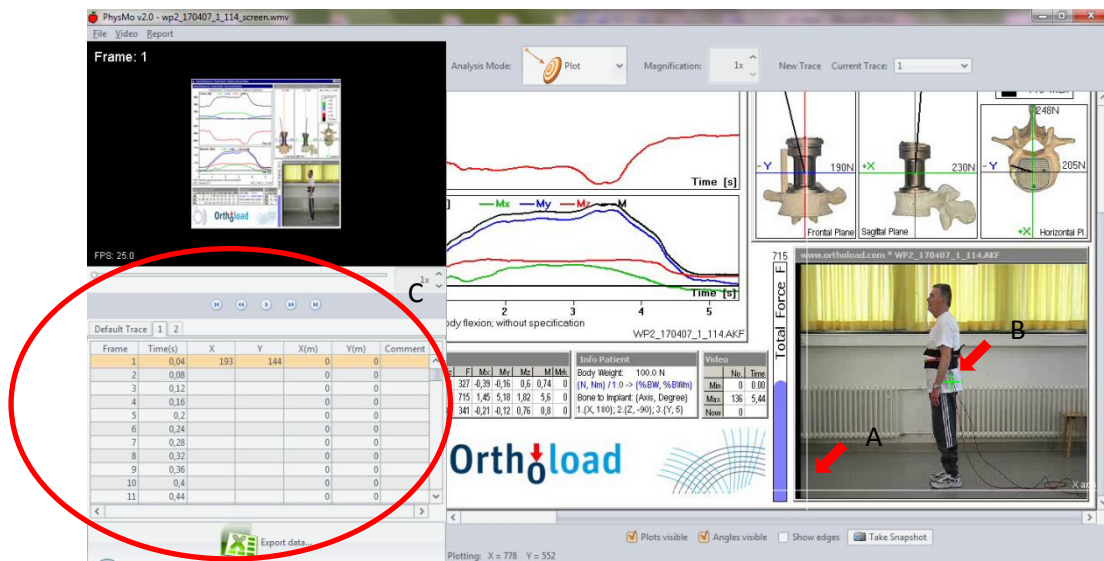
Figure 4.15 - Principal window of the software Physmo. A – Set the origin of the coordinate system. B – Position of one of the points. C – Part of the software that shows the coordinates of the study points.
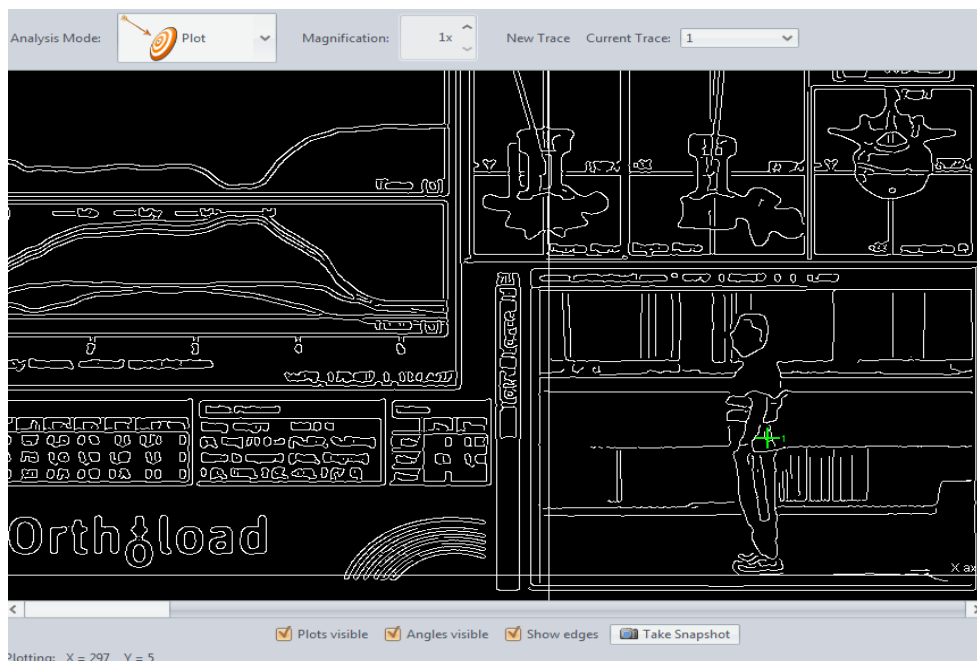
Figure 4.16 – Aspect of the video after selecting the option 'show edges'.

The coordinates of the initial and final positions were introduced into an excel document and a graph was constructed (Figure 4.17(A)). To measure the angle between the points, it was used the 'Paint' software to draw the two lines and a protractor to measure the angle (Figure 4.17(B)).
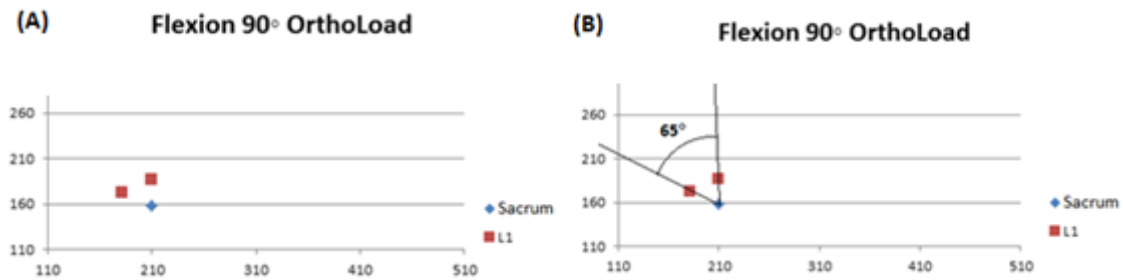
Figure 4.17 - Coordinates of the sacrum and L1 in flexion 90◦ of the patients from OrthoLoad and from the WM MBS after the Physmo analysis.

To compare the results from OrthoLoad with the MBS, the MBS was adapted to simulate a lumbar spine with a vertebral body implant. The Figure 4.18 represents one of the patients which the L1 was replaced by an implant. The implant replaced one vertebra and two intervertebral discs. To construct the VBR in WM, two coordinates were selected, each one corresponding to the geometrical center of each IVD, and the body was constructed between these two coordinates. The joint between the VBR and L2 has to be rigid and measurable.
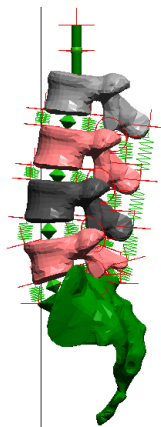
Figure 4.18 – Representation of a patient with a VBR of L1 in WM.

To reproduce the movement of the patient of OrthoLoad, it was used a file that contains the time-dependent forces and torques in the centre of the implant, from the OrthoLoad database. So, it was placed a coordinate at the centre of the body in WM and in this coordinate it was inserted 3 forces and 3 torques (that correspond to each axis: x, y and z). The forces and torque exported from the databases were introduced into the corresponding force and torque directly from the text document from OrthoLoad.

The comparison of the angles from the three movements selected with MBS can be seen at Table 4.11. To the angles measured during the flexion at 90° and during the simple flexion, it has to be subtracted the rotation of the sacrum (like it is represented at Figure 4.19).

Normal   Simple flexion   Flexion 90°
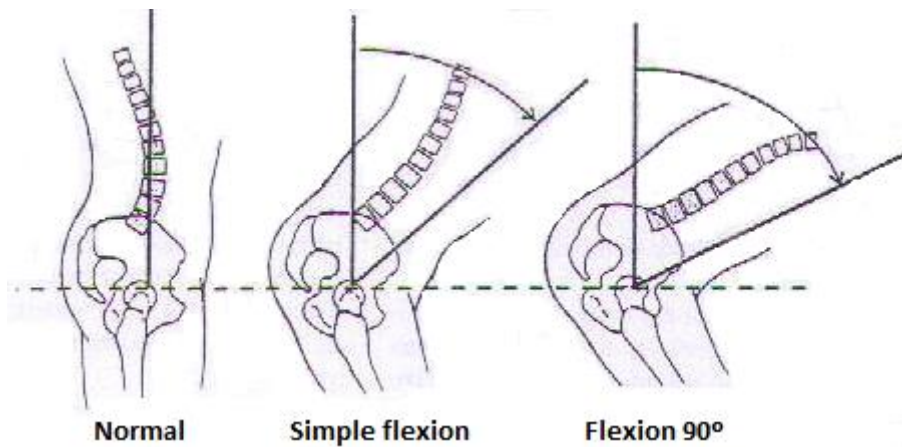
Figure 4.19 – Rotation of the sacrum during the simple flexion and the flexion at 90° {Adapted from (58)}.

Table 4.11 – Comparison of the angles for all the movements studied

Movement	Degree OrthoLoad			Degree Working Model	
	Measured	Rotation sacrum	Final angle	Without ligaments	With ligaments
Flexion 90°	65	31	34	54	16
Simple flexion	35	22	13	35	11
Extension	37	-	-	30	21
Lateral Bending	23	-	-	24	15

Interpreting the table above, the motion of the MBS without the ligaments is very similar with the movement measured with the patients of OrthoLoad without the subtraction of the sacrum's rotation. With the implementation of the ligaments, the MBS become more rigid, making the motion too small.

Chapter 5 – Application of the Model

5.1. Movement analysis

After the model validation and based on the data from OrthoLoad, some characteristics during the movement that are not feasible *in vivo*, were analyzed, like the force and torque that each IVD is subjected during a movement.

The middle of the superior end-plate of L1 was the chosen localization to the application of forces and torques. Seven situations were simulated: relax, flexion 90∘, simple flexion, lateral bending, axial rotation, compression and traction. The value of the force and torque of each movement can be found at Table 5.1. The values used were based on the maximum force/torque measured by the implants from OrthoLoad and on the work of McGlashen and his co-workers.

Table 5.1 – Force and torque applied on L1 during each movement

Movement	Force (N)	Torque(Nm)	Reference
Relax	0	0	-
Flexion 90º	164.45	4.6	OrthoLoad
Flexion	108.92	1.4	OrthoLoad
Extension	-108.92	-1.4	OrthoLoad
Left Lateral bending	81.54	3.79	OrthoLoad
Right Lateral Bending	-81.54	-3.79	OrthoLoad
Left Axial rotation	0	15.7	(55)
Right Axial Rotation	0	-15.7	(55)
Compression	320	0	(55)
Traction	-320	0	(55)

The forces and torques that each IVD is subjected during the movements selected can be seen at Figure 5.1.
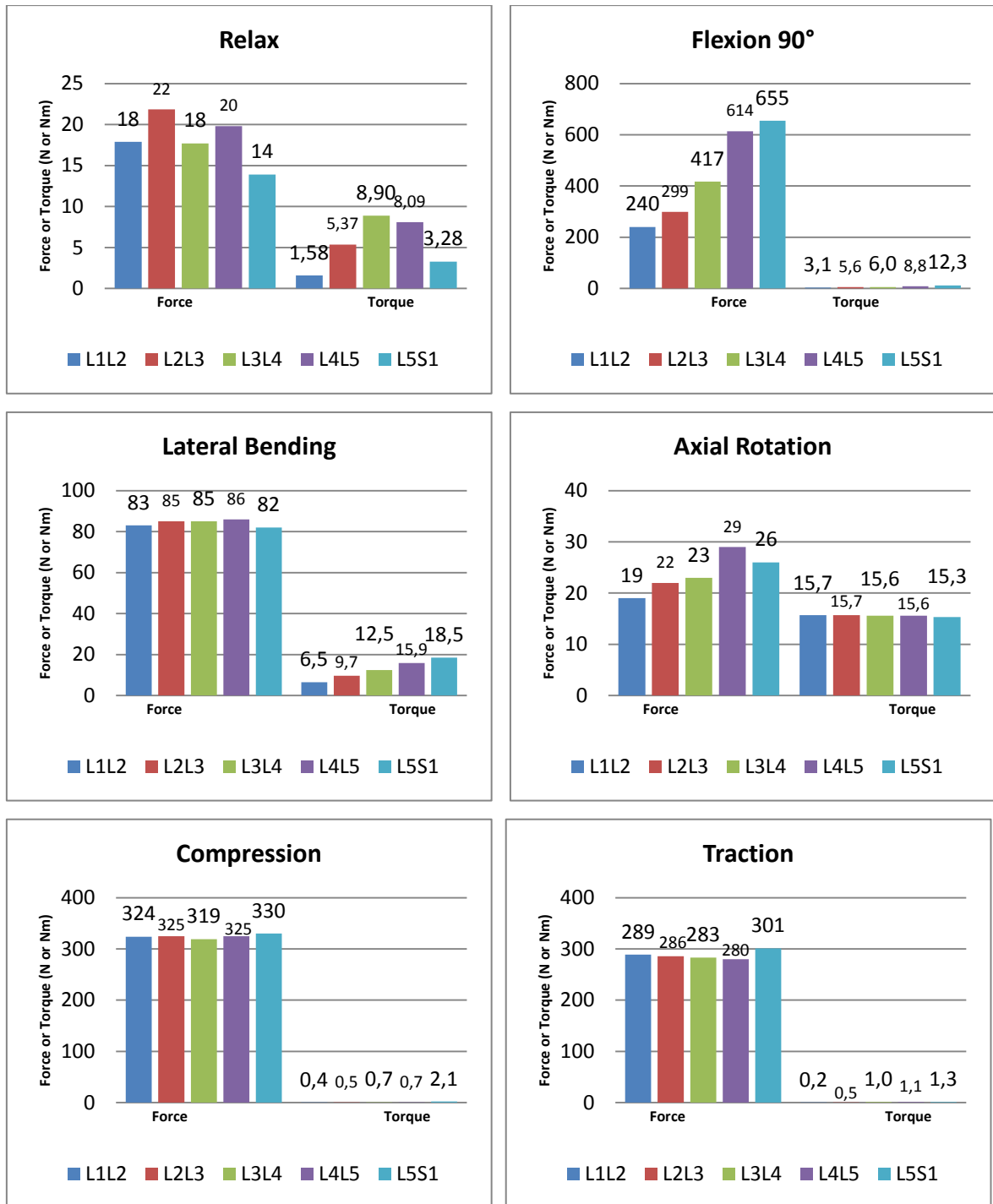
Figure 5.1 - Distribution of the force and torque along the levels during the movement studied: spine relaxed, flexion at 90º, lateral bending, axial rotation, compression and traction.

From the Figure 5.1 it is clear that the torques and forces are not distributed equally along the lumbo-sacral IVDs during the simulated movements.

When the MBS is relaxed, that is, when any force and torque is acting on the superior end-plate of L1, the IVDs are subjected to forces and torques resulting from the tension of the ligaments. The

forces are around 20N for all the levels, and the torque increases with the levels until reaching the maximum at L3L4 level, and then decreases.

During the flexion, the force increase progressively along the levels. The literature states that the lower lumbar level (L4L5 and L5S1) is the area that bears highest loads (5) (58) and the MBS is in accordance with the literature. The lower lumbar level presents higher force (almost the triple). Besides the force, the torque also increases progressively reaching the maximum at the lower lumbar levels.

The forces are divided equally along the levels, during the lateral bending. The torque increases progressively along the levels reaching a maximum at the lower lumbar levels.

During the axial rotation, the force increases progressively along the levels, reaching a maximum at level L4L5 and then decrease slightly. The torque is divided equally from L1L2 to L5S1.

The force that each IVD is subjected during the compression is almost the same for all the levels. The torque increases slightly from L1L2 to L5S1.

Like what happens during the compression, the forces that each IVD is subjected during the traction are practically the same. Once again, the torque increases slightly along the levels.

The Figure 5.2 compares the force/torque that each IVD is subjected during a symmetric movement: flexion and extension.
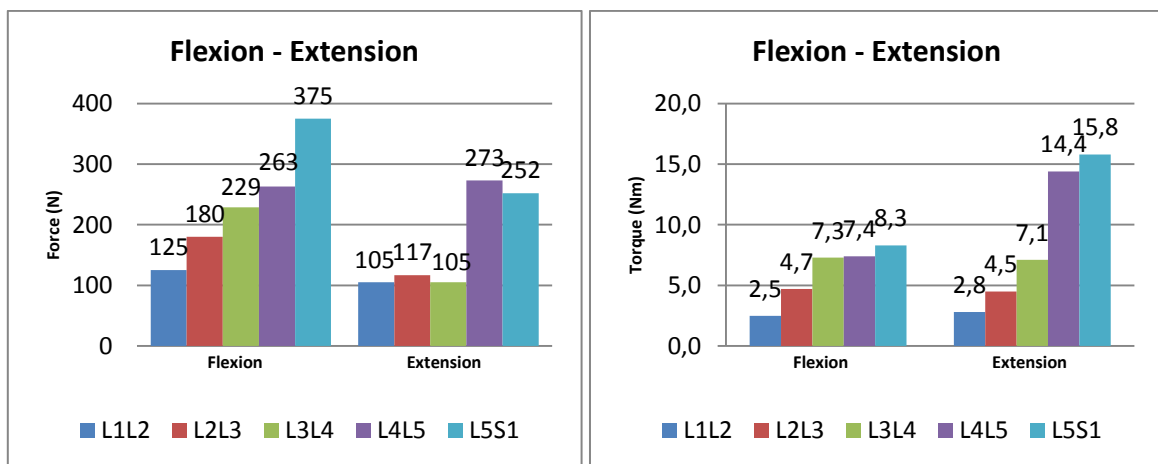
Figure 5.2 - Comparison of the force/torque at each IVD during the flexion and extension.

Interpreting the Figure 5.2, during the flexion-extension with the same force and torque but symmetric, the forces and torques that the IVDs are subjected are not the same. In all the levels, the force is smaller during the extension than during the flexion. During the flexion, the force increase progressively along the levels, while during the extension, the force is practically constant during the

three firsts lumbar levels, and then increases significantly. The torque that each IVD is subjected increases progressively along the levels during the flexion and extension, but the values are higher during the extension. It is possible to say that during the flexion there is a higher resistance to rotation of the IVD comparing with the extension. This resistance is in accordance with the movement obtained during the model validation, where the rotation of all the vertebrae during the extension is higher than during the flexion, especially for the lower lumbar levels.

5.2. Application of the analysis of diseased spine

5.2.1. Degeneration of the intervertebral disc

During aging, the demarcation between the annulus and the nucleus becomes less obvious and the nucleus pulposus loses its gel-like appearance to a fibrotic appearance.

The disc degeneration starts with a small injury in the annulus fibrosus causing damage to the nucleus pulposus. This damage causes the loss of proteoglycan and matrix disorganization. Consequently, the osmotic pressure of the disc decrease and the disc is less able to maintain hydration under load. When loaded, the IVD it lose height and fluid more rapidly, the end-plate and the annulus are subjected to inappropriate stress concentration, affecting the spinal behavior (59).

According to Thomson *et al* (60) there are five stages of the intervertebral disc degeneration, and the morphologic changes over the stages are summarizes at Table 5.2.

Table 5.2 – Description of the Nucleus pulposus, Annulus fibrosus, end-plate, vertebral body and real photographs along the intervertebral disc degeneration grades {Adapted from (60)}

Grade	Nucleus pulposus	Annulus fibrosus	End-plate	Vertebral body
I	Bulging gel	Discrete fibrous lamellas	Hyaline, uniformly thick	Margins rounded
II	White fibrous tissue peripherally	Mucinous material between lamellas	Thickness irregular	Margins pointed
III	Consolidated fibrous tissue	Extensive mucinous infiltration; loss of annular-nuclear demarcation	Focal defects in cartilage	Early osteophytes at margins
IV	Horizontal clefts parallel to end-plate	Focal disruptions	Fibrocartilage extending from subchondral bone;	Osteophytes less than 2mm

			irregularity and focal sclerosis in subchondral bone	
V	Clefts extend through nucleus pulposus and annulus fibrosus		Diffuse sclerosis	Osteophytes greater than 2mm

At the Figure 5.3 it is possible to see real photographs of the different stages of intervertebral disc degeneration.
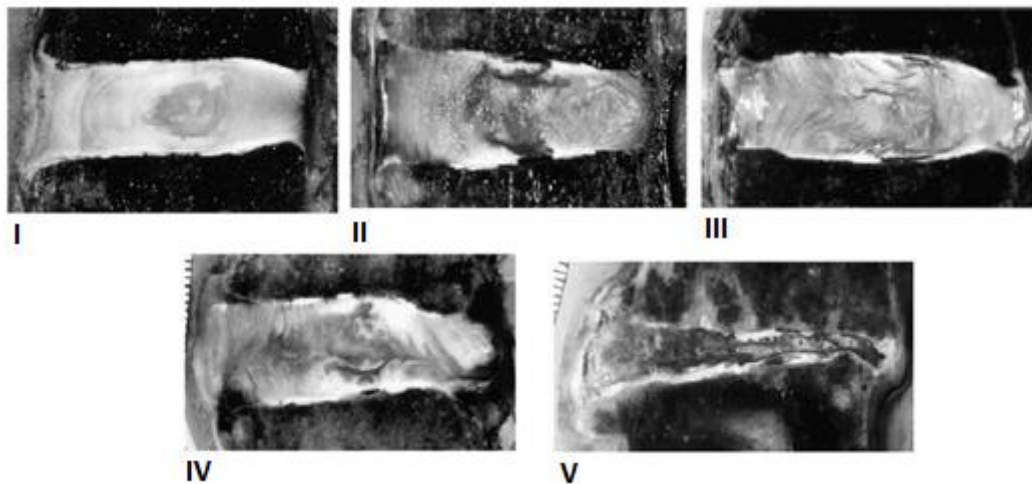
Figure 5.3 – Photographs of the five stages of intervertebral disc degeneration {Adapted from (61)}.

The higher incidence of clinically evident disc disease is at L4L5 and L5S1 due to mechanical loads that they bear in this area. Comparing with the remaining levels, the forces that the lower lumbar levels are subjected are significantly higher.

5.2.2. Treatments

They are two ways for treatment for intervertebral disc degeneration or decrease the pain related with the disease: the common nonsurgical and surgical treatment.

The nonsurgical treatments include exercise, physical therapy and medication. They are essential to relieving the pain of degenerative disc disease.

When the degeneration is more severe and the activity of the patient is limited, the surgical treatment is usually the recommended. There are three techniques for the treatment for the lumbar disc degeneration: fusion, intradiscal electrothermal therapy and disc replacement.

Fusion techniques aims to correct the existing mechanical deformation, provide stability to the segment, diminish pain, maintain the spinal curvature and promote the bone growth. There are three types of spinal fusion devices: horizontal cylinders, vertical rings and open box cages (62).

Intradiscal electrothermic therapy is a minimally invasive treatment and it involves the percutaneous threading of a flexible catheter into the disc. The catheter is composed of thermal resistive coil and is inserted at the posterior annulus fibrosus to deliver heat, causing contraction of collagen fibers and denervation of the sensory neuron of the spine (nociceptors) (63).

The disc prosthesis used for disc replacement, allows the motion between two vertebrae, prevents adjacent segment degeneration and contributes for the long-term spine stability. But similarly with other prosthetic devices, the clinical outcomes are unknown for the majority of disc (63). The prostheses are composed by three parts: two plates mimicking the end-plates and one deformable central core made of gel that can simulate the biomechanics of the intervertebral disc (64). On the market there are numerous types of disc prostheses available and prostheses designs under study or in development. The four main companies of disc prosthesis are Spine Art, Synthes, FH Orthopedics and B| Braun (14).
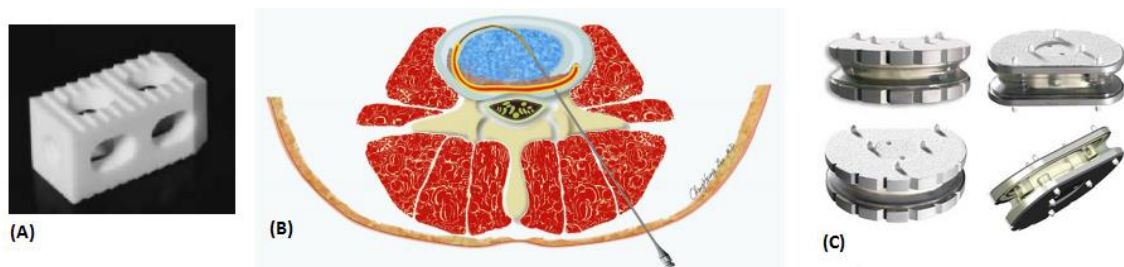
Figure 5.4 – Solutions for the intervertebral disc degeneration. (A) Prosthesis for the spinal fusion {Adapted from (65)} (B) Exemplification of the intradiscal electrothermic therapy {Adapted from (66)}. (C) Disc replacement prosthesis {Adapted from (64)}.

5.2.3. Application of spinal fusion simulation

In order to analyze the forces and torques that each IVD is subjected with a fused functional spine unit, it was decided to simulate a lumbar spine with the level L4L5 fused. For that, the bushing element representing the IVD was substituted by a rigid joint. The movements tested were: flexion, extension, lateral bending and axial rotation. The forces and torques used in each movement were higher than the ones used in the healthy spine, because the objective is to study the force/torques that each IVD is subjected during the same total movement and not the torque/force that causes the

movement. Besides the movement simulated, it was also simulated an increased movement of 150% and measured the forces and torques in each IVD, also.

Two comparisons were made: the percentage of variation of force/torque of the fused spine relatively with the normal spine during the 'normal' movement and the movement increased 150%; and the percentage of increase of force/torque of the increased movement relatively with the spine with the 'normal' movement, of the two simulated spine.

The Figure 5.5 shows the two comparisons made during the flexion.
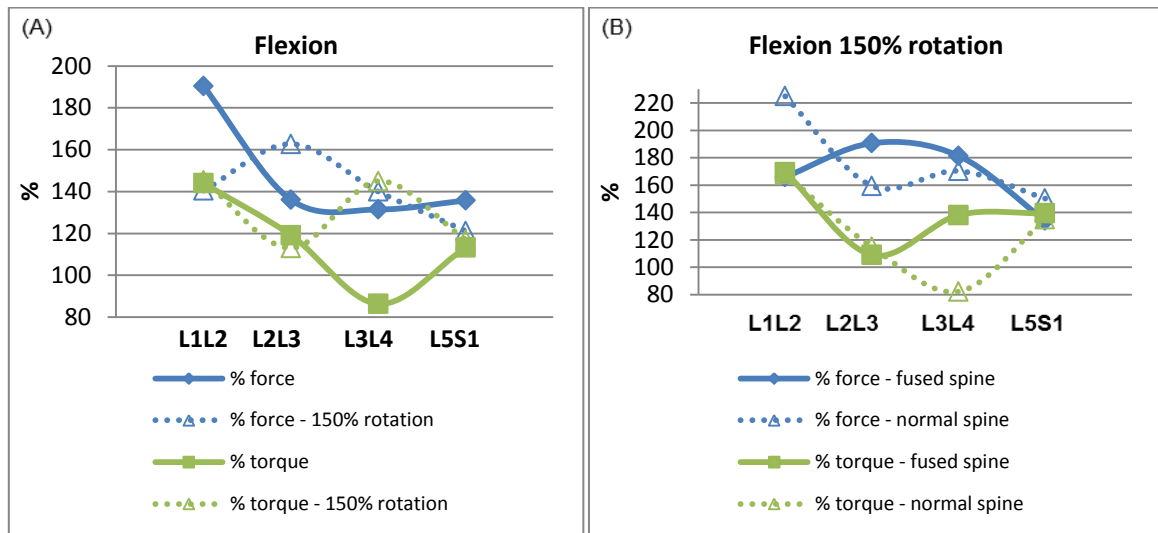
Figure 5.5 – Comparisons during the flexion: (A) percentage of force and torque of the fused spine relatively with the healthy spine. (B) percentage of the force and torque of the increased movement of the healthy and the fused spine relatively with the spine with the 'normal' movement.

From the Figure 5.5(A), it is possible to see that the force and torque of the fused spine is always higher (with the two tested rotations: 'normal' and increased) except the torque during the rotation increased 150%, at level L3L4, but the percentage difference is not significant. The level that is subjected to the highest force is L1L2 and L2L3 for the 'normal' movement and increased movement, respectively. About the torque, the value is similar in the two tested movements, but the level L3L4 (level predecessor to the fused level) presents the lower and higher value for the 'normal' movement and increased movement, respectively. It was expected that the neighboring levels of the fused level was subjected to higher force/torque, but only on the increased movement that happens for the torque at level L3L4.

The Figure 5.5(B) aims to compare the percentage variation of the force/torque along the levels of the increased movement relatively to the 'normal' movement. In both simulated spine, the force and torque is always higher during the increased movement (as it was expected) except for the torque at level L3L4, for the healthy spine. This comparison was made to see if the force/torque

variation in the healthy spine was the same in the fused spine, but they are not similar, especially for the force.

The Figure 5.6 present the comparisons made during the extension.
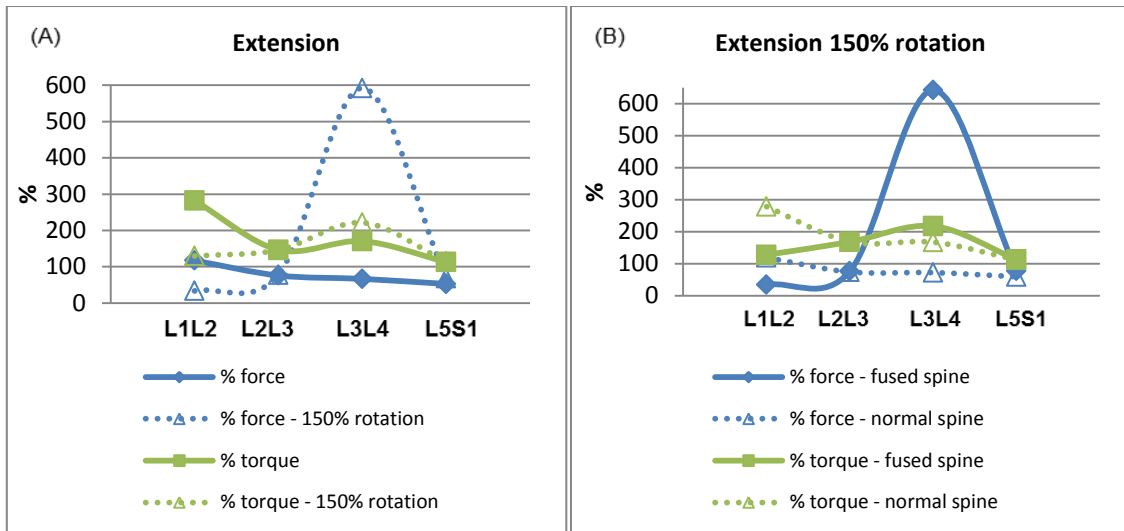
Figure 5.6 - Comparisons during the extension: (A) percentage of force and torque of the fused spine relatively with the healthy spine. (B) percentage of the force and torque of the increased movement of the healthy and the fused spine relatively with the spine with the 'normal' movement.

During the extension, the forces that the IVDs are subjected on the fused spine are always lower than the normal spine, except for the level L3L4, where the force is 600% higher for the increased movement (Figure 5.6(A)). About the torque, it is always higher in the fused spine, with an increase of value for the level L3L4, for both movements.

Interpreting the Figure 5.6(B), it is possible to see that the variation of torque for both simulated spine, are very similar during the increased movement, except for the first lumbar level. About the force variation, they are always lower during the increased movement relatively to the 'normal' movement, except for the fused spine at level L3L4, where the force is around 600% higher. About the variation along the level, they have two levels where the force percentage is the same in both spine (L2L3 and L5S1).

The Figure 5.7 shows the two comparisons made during the lateral bending.
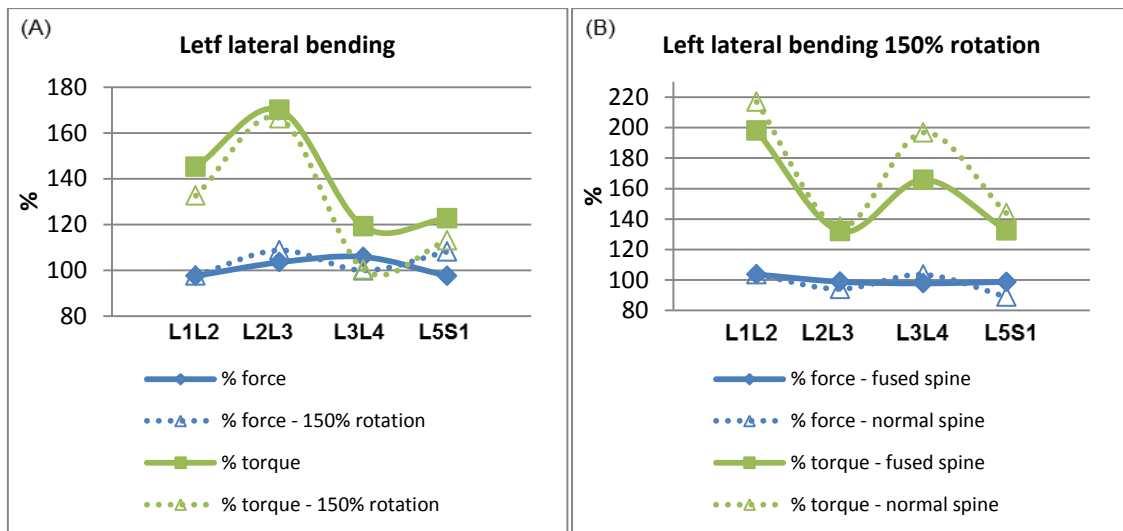
Figure 5.7 - Comparisons during the lateral bending: (A) percentage of force and torque of the fused spine relatively with the healthy spine. (B) percentage of the force and torque of the increased movement of the healthy and the fused spine relatively with the spine with the 'normal' movement.

Interpreting the Figure 5.7(A), the first aspect that is highlighted, is that the increase of force/torque in the fused spine is very similar in all the levels in both simulated movements. About the force, it is not very different than the healthy spine, in some levels (L1L2 for example), the force that the IVD is subjected is the same with or without the fusion of L4L5. The torque is higher than the normal spine in both movements and with values similar for the fused spine. Unlike what it was expected, the levels that are closest to the fused level are the levels with the lowest torque values.

On the other hand, from the Figure 5.7(B), it is possible to see that the variation of force/torque during the increased movements is very similar between the two simulated spines. The force during the increased movement was very similar to the force that each IVD was subjected during the 'normal' movement. The same did not happen with the torque, where there is an increase of torque in all the level, especially at level L1L2 and L3L4.

The Figure 5.8 present the comparisons made during the axial rotation.
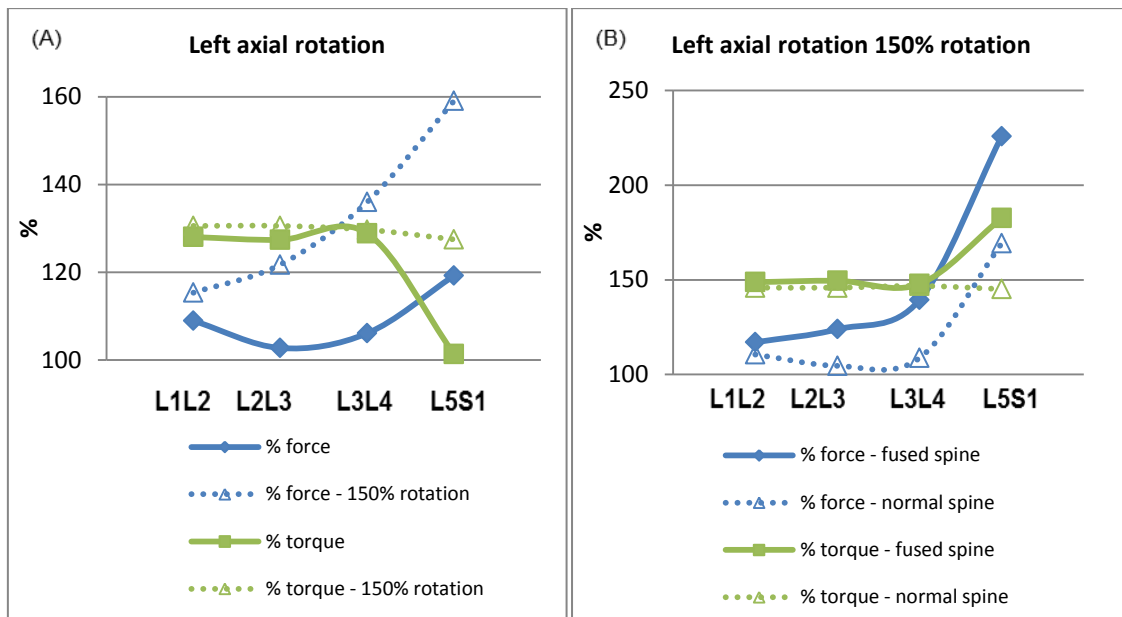
Figure 5.8 - Comparisons during the lateral bending: (A) percentage of force and torque of the fused spine relatively with the healthy spine. (B) percentage of the force and torque of the increased movement of the healthy and the fused spine relatively with the spine with the 'normal' movement.

During the axial rotation, the fused spine presents always higher force and torque than the healthy spine. The torque is very constant along the level (during the 'normal' and increased movement), except for the L5S1 level during the 'normal' movement, where the torque was equal to the healthy spine. About the force along the level it increases progressively from L1L2 to L5S1. The increased movement causes higher forces on the IVDs than the 'normal' movement.

Interpreting the Figure 5.8(B), it is possible to see that the variation of the force is different for the both simulated spine, but it is always higher during the increased movement than during the 'normal' movement. The fused spine presents higher variation than the normal spine. About the variation of torque, it is also higher during the increased movement than the 'normal' movement, for both simulated spine. For both simulated spine, the torque variation is very similar during the increased movement, except for the level L5S1.

5.2.4. Simulation of the intervertebral disc degenerated

A simulation of the IVD degenerated was planned, but due to the lack of time it was not simulated. The objective was to analyze the force and torque distribution along the levels for several simulated movements. However some published results of the vertebrae' motion was made and it can be seen at appendix B.

Chapter 6 – Conclusion and future work

6.1. Conclusion

The present work aims to develop a three-dimensional multibody model of the lumbar spine to analyze the forces and torques' distribution along the intervertebral discs during daily movement. The objective was achieved, however, due to excessive rigidity during the flexion, the movement equation of the IVDs need to be improved.

The first stage of the present work consisted on summarise the literature review of the state-of-the-art of multibody model of the spine. The followed stage was focused on the anatomy of the spine, where it was descripted the principal elements for the development of the model, the spinal movement and spinal disorders (especially the disc degeneration).

After the first stage, the multibody model was developed consisting on six vertebra (L1 to S1), six intervertebral discs, ligaments and facet joints. The vertebrae were simulated as rigid bodies, the intervertebral discs as bushing elements, the ligaments as spring element and the facet joints as separators. From the finite element analysis it was possible to have the motion equations, and from them the spring constant of the bushing elements were characterized. The vertebrae were simulated as rigid bodies and the value of their masses and localization were found in the literature. The spring constant of the ligaments were characterized using curves of force-deformation from published results.

The validation of the model was made using data from the literature and data from the database of OrthoLoad. From the validation, the flexion of the multibody is more rigid than the flexion measured in the literatures, but the extension was very similar in some levels. Besides, the value of extension is always higher than the value of flexion (for the symmetric value of torque) which is not in accordance with the physiologic movements of the spine. The motion from the finite element also presents higher movement during the extension than during the flexion. So, this can be one of the reasons why the multibody also behaves unlike the physiologic movements. Besides, the spring constant of the ligaments can be too rigid and it influence of the spine flexibility. About the lateral

flexion and axial rotation, there were some differences of the rotation, especially with low values of torques.

From the movement analysis it was possible to see that during the flexion there is an increase of force from L1L2 to L5S1. The torque is constant for the three first lumbar intervertebral discs (L1L2, L2L3 and L3L4) and then increases progressively along the other levels. During the lateral bending the force also increase progressively along the levels, while the torque is constant. During the axial rotation, the force increases progressively from L1L2 to L4L5, but decreases slightly at L5S1. About the torque, it is constant along the lumbar intervertebral discs. During the compression and traction, all the levels seem to be subjected to the same forces and torques. Comparing symmetric movements, there are some differences on the force distribution during the flexion and extension. While during the flexion, the force increases progressively from L1L2 to L5S1, during the extension, the force is constant at the three first levels, and then increases progressively. About the torque, there are no differences to point.

From the movement analysis of the fused spine, at level L4L5, it was concluded that, in general, the force and torque incident in each IVD of the fused spine is similar or higher than the healthy spine. During the flexion, the force is always higher and non-constant; and there is no relation between the value of the spine rotation and the force. About the torque, it is also higher on the fused spine and constant along the levels, except for the level L3L4, where higher rotation causes higher torque. During the extension, the force on the IVDs of the fused spine is always lower than the healthy spine, except for the level L3L4, where the force increases 600%. Higher rotation of the spine decreases the force that each IVD is subjected, except for the level L3L4. About the torque, it is always higher on the fused spine and higher rotation causes lower value of torque that each IVD is subjected, except for the level L3L4. During the lateral bending, the force and torque each IVD is subjected on the fused spine is similar and higher than the healthy spine, respectively. Higher rotation of the spine does not causes any difference on the force and torque that each IVD is subjected during the lateral bending. The last movement analyzed was the axial rotation. The force that each IVD is subjected during this movement is always higher on the fused spine than on the healthy spine. Higher rotation also causes higher force on the IVDs. On the other hand, the torque is always on the fused spine and higher rotation does not cause any differences on the torque that each IVD is subjected, except for the level L5S1, where the torque is higher.

In general, the movement analysis were in accordance with the literature, where the lower lumbar levels (L4L5 and L5S1) where the levels which are subjected to higher forces. For the fused spine, the analysis is also in accordance with the expected, where the neighbor intervertebral discs are the discs that are subjected to higher force and torque, especially the level L3L4.

6.2. Future work

To complete this work, some details need to be improved to have a better simulation of the lumbar spine:

- Add the capsular and the intertransverse ligament to the multibody;
- Improve the simulation of the ligaments under compression. At the end of the work, it was noticed that the ligament, under compression, applied an opposite force and this should not happen because the ligaments don't work under compression;
- Simulate a new IVD that encompasses the posterior and anterior ligaments;
- Simulate the intervertebral disc degenerated and
- Extend the simulation to the whole human spine.

References

1. **eumusc.net.** *Musculoskeletal Health in Europe - Report v5.0.* Executive Agency for Heatlh and Consumers.

2. **Andrew Clarke, Alwyn Jones, Michael O'Malley and Robert McLaren.** *ABC of Spinal Disorders.* United Kingdom : Wiley-Blackwell, 2010. ISBN: 9781405170697.

3. **Katz, Jeffrey N.** *Lumbar Disc Disorders and Low-Back Pain: Socioeconomic Factors and Consequences.* USA : Journal of Bone and Joint Surgery, 2006, Vol. 88 Suppl2, pp. 21-24.

4. **Miguel Gouveia, Margarida Augusto.** *Custos indirectos da dor crónica em Portugal.* Lisboa : Revista Portuguesa de Saúde Pública, 2011, Vol. 29 no2.

5. **White, A. A. and Panjabi, M. M.** *Clinical Biomechanics of the Spine - Second Edition.* Philadelphia : J.B. Lippincott Company, 1990.

6. **Esat, V.** *Biomechanical Modelling of the Whole Human Spine for Dynamic Analysis.* UK : PhD Thesis, Loughborough University, 2006.

7. **Zadeh, R. S.** *A three-dimensional multibody computational model of lumbar spine.* Iran : MSc Thesis, Azad University, 2000.

8. **Monteiro, N.** *Analysis of the Intervertebral Discs Adjacent to Interbody Fusion using a Multibody and Finite Element Co-Simulation.* Lisbon, Portugal : MSc Thesis, Technical University of Lisbon, 2009.

9. **Esat, V and Acar, M.** *A Multi-Body Model of the Whole Human spine for Whiplash Investigations.* Lyon : In: 20th Enhanced Safety oh Vehicles Conference: Innovations for Safety: Opportunities and Challenges, 2007.

10. **Shirazi, A. Arjmand, N. Parnianpour, M.** *Trunk Biomechanics During Maximum Isometric Axial Torque Exertions in Upright Standing.* Canada : Journal of Clinical Biomechanics, 2008, Vol. 23(8), pp. 969-978.

11. **Monheit, G. and Badler, N.** *A Kinematic Model of the Human Spine and Torso.* USA : Technical Reports (CIS) University of Pennsylvania, 1990.

12. **Lavaste, F. et al.** *Three-Dimensional Geometrical and Mechanical Modelling of the Lumbar Spine.* France : Journal of Biomechanics, 1992, Vol. 25(10), pp. 1153-1164.

13. **Menon, R.** *Multibody and Finite Element Approaches in the Development of a Model for the Human Head-Neck-Torso System.* USA : PhD Thesis, Wichita State University, 1995.

14. **Morais, S.** *Development of a Biomechanical Spine Model for Dynamic Analysis.* Guimarães, Portugal : MSc Thesis, Unversity of Minho, 2011.

15. **Broman, H. et al.** *A Mathematical Model of the Impact Response of the Seated Subject.* Sweden : Medical Engineering & Physics, 1996, Vol. 18(5), pp. 410-419.

16. **Kitazaki, S. and Griffin, J.** *A Modal Analysis of Whole-Body Vertical Vibration, using a Finite Element Model of the Human Body.* UK : Journal of Sound and Vibration, 1997, Vol. 200(1), pp.83-103.

17. **Duque, Luiz.** *Modelo Dinâmico da Coluna Lombar Humana com Solicitação de Esforço Póstero-Anterior:Análise com Rigidez Viscoelastica Não-Linear.* Guaratinguetá : PhD Thesis Paulista Statal University, 2006.

18. **Pankoke, S. et al.** *Dynamic FE Model of Sitting Man adjustable to Body Height, Body Mass and Posture used for Calculating Internal Forces in the Lumbar Vertebral Disks.* Germany : Journal of Sound and Vibration, 1998, Vol. 215(4), pp.827-839.

19. **Stokes, I. and Gardner-Morse, M.** *Quantitative Anatomy of the Lumbar Musculature.* USA : Journal of Biomechanics, 1999, Vol. 32, pp.311-316.

20. **Jager, M.** *Mathematical Head-Neck Model for Acceleration Impacts.* Eindhoven : PhD Thesis, Eindhoven University, 2000.

21. **Lengsfel, M. et al.** *Lumbar Spine Curvature During Office Chair Sitting.* Germany : Medical Engineering & Physics, 2000, Vol. 22, pp.665-669.

22. **Keller, T. and Colloca, C.** *A Rigid Body Model of the Dynamic Posteroanterior Motion Response of the Human Lumbar Spine.* USA : Journal of Manipulative and Physiological Therapeutics, 2002, Vol. 25(8), pp.485-496.

23. **Waters, T., Li, F., Huston, R. and Kittusamy, N.** *Biomechanical Modeling of Spinal Loading Due to Jarring and Jolting for Heavy Equipment Operators.* pp.4, Korea : Proceeding of XVth Triennial Congress of the International Ergonomics Association and 7th Joint Conference of Ergonomics Society of Korea/Japan Ergonomics Society, 2003.

24. **Ishikawa, Y., Shimada, Y., Iwami, T. Kamada, K, Matsunaga, T., Misawa, A., Aizawa, T. and Itoi, E.** *Model Simulation for Restoration of Trunk in Complete Paraplegia by Functional Electrical Simulation.* Canada : Proceedings of IFESS05 Conference.

25. **Ferreira, A.** *Multibody Model of the Cervical Spine and Head for the Simulation of Traumatic and Degenerative Disorders.* Lisbon, Portugal : MSc Thesis, Technical University of Lisbon, 2008.

26. **Zang, Q. and Teo, E.** *Finite Element Application in Implant Research for Treatment of Lumbar Degenerative Disc Disease.* Singapore : Journal of Medical Engineering and Physics, 2008, Vol. 30, pp.1246-1256.

27. **Fairman, M, Ghasempoor, A. and Abdoli-E, M.** *Development of a Multibody Computational Model of the Lumbar Spine with Simulink.* Toronto : Proceeding of Science and Technology for Humanity (TIC-STH), IEEE Toronto International Conference, 2009, pp.130-133.

28. **Juchem, S. and Gruber, K.** *MBS Model for the Estimation of Forces and Torques in the Human Lumbar Spine.* Germany : Proceedings of World Congress on Medical Physics and Biomedical Engineering, 2009, pp.2234-2237.

29. **Chen, C., Cheng, C., Liu, C. and Lo, W.** *Stress Analysis of the Disc Adjacent Fusion in Lumbar Spine.* Journal of Medical Engineering and Physics, 2001, Vol. 23, pp.483-491.

30. **Christophy, M.** *A Detailed Open-Source Musculoskeletal Model of the Human Lumbar Spine.* USA : MSc Thesis, University of California, 2010.

31. **Abouhosein, A., Weisse, B. and Ferguson, S.** *A Multibody Modeling Approach to Determine Loads Sharing between Passive Elements of the Lumbar Spine.* Switzerland : Computer Methods in Biomechanics and Biomedical Engineering, 2011, Vol. 14, pp.527-537.

32. **Galibarov, P., Dendorfer, S. and Torholm, S.** *On Modelling Spine Curvature Dependent on Muscular and External Forces in Multibody Dynamic System.* Denmark : ISB Brussels, 2011.

33. **Han, K., Zander, T., Taylor, W. and Rohlmann, A.** *An Enhanced and Validated Generic Thoraco-Lumbar Spine Model for Prediction of Muscle Forces.* Germany : Medical Engineering and Physics, 2012, Vol. 34, pp.709-716.

34. **Netter, Frank H.** *Atlas de Anatomia Humana 2ed.* Porto Alegre: Artmed, 2000.

35. **Pina, J. and Esperança, A.** *anatomia Humana da Locomoção - 2a Edição.* Lisbon : Lidel, 1999. Vols. ISBN:972-9018-99-5.

36. **Ebraheim, N., Hassan, A. and Lee, M. and Xu, R.** *Functional Anatomy of the Lumbar Spine.* USA : Elsevier, 2004, pp.131-137.

37. **Walsh, J., Quinlan, J. and FizPatrick, D. and McCormack, D.** *Three-dimensional motion analysis of the lumbar spine during "free squat" weight lift training.* Ireland : Am. Journal Sports Med., 2007, Vol. 35(6), pp.927-932.

38. **Gosling, J. et al.** *Human anatomy - Color atlas and text, 3rd edition.* Hong Kong : Mosby-Wolfe, 1996. Vol. ISBN: 0 7234 2657 0.

39. **Bogduk, N.** *Clinical Anatomy of the Lumbar Spine and Sacrum - Fourth Edition.* Australia : Elsevier Churchill Livingstone, 2005.

40. **Jensen, G.** *Biomechanics of the Lumbar Intervertebral Disk: A Review.* USA : Journal of the American Physical Therpy Association, 1980, Vol. 60(6), pp.765-773.

41. **Faller, A. and Schuenke, M.** *The Human Body - An Introduction to Structure and Function.* New York : Thieme, 2004. Vols. ISBN: 1-58890-122-X (TNY).

42. **Moramarco, V., Palomar, A. and Pappalettere, C. and Doblaré, M.** *An accurate valitadion of a computational model of a human lumbosacral segment.* Spain : Journal of Biomechanics, 2009, Vol. 43, pp.334-342.

43. **Dumas, G. and Beaudoin, L. and Drouin, G.** *In Situ Mechanical Behavior of Posterior Spinal Ligaments in the Lumbar Region, an In Vitro Study.* Canada : Journal Biomechanics, 1986, Vol. 20(3), pp.301-310.

44. **Médicos de Portugal.** *Dossier Informativo - Doenças da Coluna.* 2008.

45. **Flores, P. and Seabra, E.** *Dynamics of Planar Multibody Systems.* Guimarães : Escola de Engenharia, Universidade do Minho, 2011.

46. **WorkingModel.** *Working Model (R) 3D - User's Manual. Version 3.0.* USA : Knowledge Revolution, 1997.

47. **Keller, T. and Colloca, C. and Béliveau, J.** *Force-deformation response fo the lumbar spine: a sagittal plane model of posteroanterior manipulation and mobilization.* USA : Clinical Biomechanics, 2002, Vol. 17, pp.185-196.

48. **Chazal, J. et al.** *Biomechanical properties of spinal ligaments and histological study of the supraspinal ligament in traction.* France : Journal of Biomechanics, 1985, Vol. 18(3), pp.167-176.

49. **Robertson, D. and Forell, G. and Bowden, A.** *Thoracolumbar spinal ligament exhinit negative and transverse pre-strain.* USA : Journal of the Mechanical Behavior of Biomedical Materials, 2013.

50. **Hukins, D. et al.** *Comparison of structure, mechanical properties, and functions of lumbar spinal ligaments.* UK : Spine, 1990, Vol. 15(8), pp.787-795.

51. **Tkaczuk, H.** *Tensile properties of human lumbar longitudinal ligaments.* Acta Orthopaedica Scand., 1968, Vol. 115[Suppl.].

52. **Nachemson, A. and Evans, J.** *Some mechanical properties of the third human lumbar interlaminar ligament (ligamentum flavum).* UK : Jornal of Biomechanics, 1968, Vol. 1, pp.211-220.

53. **Weishaupt, D., Zanetti, M. and Boos, N. and Hodler, J.** *MR imaging and CT in osteoarthritis of the lumbar facet joints.* Switzerland : Skeletal Radiol., 1999, Vol. 28, pp.215-219.

54. **Panjabi, M., Oxland, T. and Yamamoto, I. and Crisco, J.** *Mechanical Behavior of the Human Lumbar and Lumbosacral Spine as Shown by Three-Dimensional Load-Displacement Curves.* New Haven : The Journal of Bone and Joint Surgery, 1994, Vols. 76-A (3), pp.413-423.

55. **Guan, Y. et al.** *Moment-rotation responses of the human lumbosacral spinal column.* USA : Journal of Biomechanics, 2007, Vol. 40, pp.1975-1980.

56. **McGlashen, K., Miller, J. and Schultz, A. andAndersson, G.** *Load displacement behavior of the human lumbo-sacral joint.* USA : Journal of Orthopaedic Research, 1987, Vol. 5, pp.488-496.

57. **www.orthoload.com.**

58. **Knutzen, Joseph Hamill and Kathleen.** *Bases biomecânicas do movimento humano.* Editora Manole Ltda, 1999.

59. **Miller, J. and Schmatz, C. and Shultz A.** *Lumbar disc degeneration: correlation with age, sex, and spine level in 60 autopsy specimens.* USA : Spine, 1988, Vol. 13(2) pp.173-178.

60. **Urban, J. and Roberts, S.** *Degeneratio of the intervertebral disc - Review.* UK : Arthritis Research & Therapy, 2003, Vol. 5(3), pp.120-130.

61. **Thomson, J. et al.** *Preliminary Evalutation of a Scheme for Grading the Gross Morphology of the Human Intervertebral Disc.* Canada : Spine, 1990, Vol. 15(5), pp.411-415.

62. **Tanaka, N. et al.** *The relationship between disc degeneration and flexibility of the lumbar spine.* USA : The Spine Journal, 2001, Vol. 1, pp.47-56.

63. **Chou, Y. et al.** *Efficacy of anterior cervical fusion: comparison of titanium cages, polyetheretherketone (PEEK) cages and auytogenous bone grafts.* Taiwan : Jounal Clinical Neuroscience, 2008, Vol. 15(11), pp.1240-1245.

64. **An, H. et al.** *Emerging Techniques for Treatment of Degenerative Lumbar Disc Disease.* Spine, 2003, Vol. 28(15S), pp.24-25,

65. **Lazennec, J. et al.** *The LP-ESP(R) lumbar disc prosthesis with 6 degrees of freedom: development and 7years of clinical experience.* France : Eur Journal Orthop Surg Traumatol., 2013, Vol. 23(2), pp.131-143.

66. **Shikinami, Y. and Okuno, M.** *Mechanical evaluation of novel spinal interbody fusion cages made of bioactive, resorbable composites.* Japan : Biomaterials, 2003, Vol. 24, pp.3161-3170,

67. **Derby, R., Baker, R. and Lee, C. and Anderson, P.** *Evidence-informed management of chronic low back pain with intradiscal electrothermal therapy.* USA : The Spine Journal, 2008, Vol. 8, pp.80-95.

68. **Rozumalski, A. et al.** *The in vivo three dimensional motion of the human lumbar spine during gait.* USA : Gait & Posture, 2008, Vol. 28, pp.378-384.

69. **Xia, Q. et al.** *In-vivo motion characteristics of lumbar vertebrae in sagittal and transverse planes.* USA : Journal of Biomechanics, 2010, Vol. 43, pp.1905-1909.

70. **Takayanagi, K. et al.** *Using Cineradiography for Continuous Dynamic-Motion Analysis of the Lumbar Spine.* Japan : Spine, 2001, Vol. 26(17), pp.1858-1865,

71. **Shirazi-Adl, A.** *Biomechanics of the umbar spine in sagittal/lateral moments.* Canada : Spine, 1994, Vol. 19(21), pp.2407-2414.

72. **Powers, C., Kilug, K. and Harrison, J. and Bergman, G.** *Segmental mobility of the lumbar spine during a posterior to anterior mobilization_ assessment using dynamic MRI.* USA : Clinical Biomechanics, 2003, Vol. 18, pp.80-83.

73. **Ochia, R. et al.** *Non-invasive assessment of in vivo kinematics of the lumbar spine.* Chicago : Conference SEM x International Congree & Exposition on Experimental & Applied Mechanics, 2004.

74. **Ibarz, E. et al.** *Development and Kinematic Verification of a Finite Element Model for the Lumbar Spine: Application to Disc Degeneration - Research Article.* Spain : Hindawi Publishing Corporation, 2012.

75. **Little, J.M Pearcy, M. and Adam, C.** *Coupled rotations in the lumbar spine- are these a consequence of passive spinal anatomy?* United Kingdom : Eds. Proceedings 7th International conference on Modelling in Medicine and Biology, 2007.

76. **Svedmark, P.** *Assessment of 3D movements in the Lumbar and Cervical spine with a net CT based method.* Stockholm : PhD Thesis Karolinska Institutet, 2011.

77. **Wheeler, D. et al.** *Inter-laboratory variability in in vitro spinal segment flexibility testing.* USA : Journal of Biomechanics, 2011, Vol. 44, pp.2383-2387.

78. **Park, W. and Kim, Y. and Lee, S.** *Effect on intervertebral disc degeneration on biomechanical behaviors of a lumbar motion segment under physiological loading conditions.* Korea : Journal of Mechanical Science and Technology, 2013, Vol. 27(2), pp.483-489.

79. **McGregor, A. and Cattermole, H. and Hughes, S.** *Spinal motion in lumbar degenerative disc disease.* UK : The Journal of Bone and Joint Surgery, 1998, Vols. 80-B (6), pp.1009-1013.

80. **Fujiwara, A. et al.** *The effect of disc degeneration and facet osteoarthritis on the segmental flexibility of the lumbar spine.* USA : Spine, 2000, Vol. 25(23), pp.3036-3044.

81. **Modic, M. and Ross, J.** *Lumbar Degenerative Disck Disease - Review.* Cleveland : Radiology, 2007, Vol. 245(1), pp.43-61.

Appendix A – Range of motion of the lumbar vertebrae

The table 1 summarizes the published data of the limits and the range of motion of the lumbar vertebrae.

Table 1 - Summary of the limits and range of motion (of the six degree of freedom) of the lumbar spine found in the literature

Reference	Level	Force	Localization	Translation (mm)			Rotation (degree)					
				Coronal	Sagittal	Transverse	Lateral Flexion		Flexion_Extension		Axial rotation	
							Left	Right	Flexion	Extension	Left	Right
(39)	L1-L2	-					5.00	6.00	8	5	1	1
	L2-L3	-					5.00	6.00	10	3	1	1
	L3-L4	-					5.00	6.00	12	1	1	2
	L4-L5	-					3.00	5.00	13	2	1	2
	L5-S1	-					0.00	2.00	9	5	1	0
(70)	L1-L2	-					10.97 (3.85)		14.38 (6.09)		8.05 (3.37)	
	L2-L3	-					14.60 (4.86)		16.72 (6.29)		7.89 (4.35)	
	L3-L4	-					14.32 (4.63)		17.72 (5.12)		6.91 (2.04)	
	L4-L5	-					10.57 (4.57)		16.87 (4.74)		7.55 (5.03)	
	L5-S1	-					7.91 (3.47)		14.33 (6.64)		7.22 (5.02)	
(71)	L2-L3	-			-0.6	0.7 +- 0.4			6.8 +- 2.9		3.2 +- 1.9	
	L3-L4	-			-0.9	1.0 +- 0.9			6.7 +- 2.3		2.8 +- 1.7	
(72)	L2-L3	-			3.15 (max) 0.1 (min)				6 (max) 0 (min)			
	L3-L4	-			3.10 (max) 0.31 (min)				6.68 (max) 1.25 (min)			
	L4-L5	-			2.1 (max) 0.78 (min)				5.12 (max) 2 (min)			
	L5-S1	-			0.57 (max) 0.73 (min)				2.37 (max) 1.43 (min)			

	L1-L2	10 Nm	L1				5 +- 1.4	8.8 +- 2.4		
	L2-L3	10 Nm	L1				6 +- 1.2	10.8 +- 2.4		
(54)	L3-L4	10 Nm	L1				5.2 +- 1.9	10 +- 3.8		
	L4-L5	10 Nm	L1				4.8 +- 2.9	12.8 +- 4		
	L5-S1	10 Nm	L1				4.4 +- 2.2	14.8 +- 4		
	L1-L2	10 Nm	L1				5.2	10.4		
	L2-L3	10 Nm	L1				5.8	10.8		
(73)	L3-L4	10 Nm	L1				6	12.5		
	L4-L5	10 Nm	L1				5.7	13		
	L5-S1	10 Nm	L1				3	10.2		
	L1-L2							- 2.1 +- -1.6		
	L2-L3							-0.5 +- -1.8		
	L3-L4		L1					1.2 +- 1.8		
	L4-L5							1.4 +- 2.4		
	L5-S1							1.2 +- 2.7		
	L1-L2							-2.1 +- -1.4		
	L2-L3							-1.4 +- -2.4		
	L3-L4		L2					0 +-1.7		
(74)	L4-L5	2.25 - 2.85 Nm						0.2 +- 1.9		
	L5-S1							1.2 +- 1.8		
	L1-L2							-0.6+- -1.4		
	L2-L3							-0.9 +- -1.2		
	L3-L4		L3					-2 +- -2		
	L4-L5							-1.7 +- -2		
	L5-S1							-1.2 +- -2.6		
	L1-L2							-0.2 +- -0.6		
	L2-L3		L4					-07 +- -1.4		
	L3-L4							-1 +- -1.3		

	L4-L5						-2.3 +- -1.4	
	L5-S1						-1.2 +- -2.4	
	L1-L2						-0.1 +- -2.6	
	L2-L3						-90.1 +- -1.6	
	L3-L4	L5					-0.8 +- -2.5	
	L4-L5						-1.4+- -2.3	
	L5-S1						-3 +- -2.2	
(75)	L1	Rotation Right 50°	-2.7	-10.83	-1.66	4.61	-0.76	-16.53
	L2		-2.5	-6.25	-1.25	2.88	-0.38	-14.61
	L3		-2.7	-2.91	-1.25	1.15	-0.19	-11.73
	L4		-2.5	-0.83	-1.04	-0.38	0	-9.42
	L5		-2.08	-1.66	-0.83	0	-0.57	-9.23
	S1		-0.83	-3.75	-0.41	0.1	0	-7.11
	L1	Rotation Right 30°	-0.41	-4.37	-0.62	3.46	0.38	-9.42
	L2		-0.83	-2.5	-0.41	2.11	0.57	-8.65
	L3		-1.04	-0.2	-0.2	0.76	0.57	-6.53
	L4		-1.25	0.41	-0.1	-0.38	0.65	-4.61
	L5		-1.04	0.3	0	-0.19	0.19	-4.23
	S1		-0.62	-1.04	0.1	0	0	-3.26
	L1	Rotation Left 30°	-5	7.29	-1.25	-3.07	-0.57	8.84
	L2		-5.2	4.37	-1.04	-1.92	-0.76	7.69
	L3		-4.58	2.91	-1.04	-0.76	-0.96	6.15
	L4		-3.75	1.87	-0.83	0	-1.15	5
	L5		-2.5	1.66	-0.83	-0.57	-1.15	4.23
	S1		-1.66	2.29	0	-0.38	-0.96	3.07
	L1	Rotation Left 50°	-6.87	17.08	-2.08	-3.84	-1.15	16.53
	L2		-7.29	12.5	-2.29	-2.3	-1.15	14.8
	L3		-6.25	8.95	-2.29	-1.15	-1.92	1.69

						Mean	Lower/Upper	Mean	Lower/Upper	Mean	Lower/Upper
	L4		-5	6.87	-1.87	-0.57		-1.92		10.38	
	L5		-2.91	6.25	-1.66	-1.15		-2.11		9.42	
	S1		-0.41	7.08	-0.2	-0.5		-1.73		8.46	
(5)	L1-L2	In vitro				4.9	3.8/6.5	10.7	5/13	2.1	0.9/4.5
	L2-L3					7	4.6/9.5	108	8/13	2.6	1.2/4.6
	L3-L4					5.7	4.5/8.1	11.2	6/1	2.6	0.9/4
	L4-L5					5.7	3.2/8.2	14.5	9/20	2.2	0.8/4.7
	L5-S1					5.5	3.9/7.8	17.8	10/24	1.3	0.6/2.1
(5)	L1-L2	in vivo/active				5.5	4/10	7	1/14	1	-1/2
	L2-L3					5.5	2/10	9	2/16	1	-1/2
	L3-L4					5	3/8	10	2/18	1.5	0/4
	L4-L5					2.5	3/6	13	2/20	1.5	0/3
	L5-S1					1	1/6	14	2/27	0.5	-2/2
(5)	L1-L2	in vivo/active				7.9	14.2	13	3/23		
	L2-L3					10.4	16.9	14	10/18		
	L3-L4					12.4	21.2	13	9/17		
	L4-L5					12.4	19.8	16	8/24		
	L5-S1					9.5	17.6	14	4/24		
(5)	L1-L2	in vivo/passive						11.9	8.6/17.9		
	L2-L3							14.5	9.5/19.1		
	L3-L4							15.3	11.9/21		
	L4-L5							18.2	11.6/25.6		
	L5-S1							17	6.3/23.7		
(5)	L1-L2					6	3/8	12	9/16	2	1/3
	L2-L3					6	3/9	14	11/8	2	1/3
	L3-L4					8	5/10	15	12/18	2	1/3

	L4-L5					6	5/7	17	14/2	2	1/3
	L5-S1					3	2/3	20	18/22	5	3/6
(76)	L1					23.4 +- 2.39		33.98 +- 4.91		38.73+-4.29	FE model 10
	L2					20.08 +- 2.55		30.25 +- 3.93		34.17+-4.29	7.25
	L3					16.12 +- 1.38		24.78 +- 6.2		31.70+-4.28	4.75
	L4					9.45 +- 1.33		18.09 +- 6.83		24.25+-5.24	2.75
	L5					4.21 +- 0.63		9.69 +- 4.5		12.66+-4.06	0.87
(77)	L1-L2					6 +- 2	-5 +- 2	-8 +- 5	5 +- 2	1 +- 1	-1 +- 1
	L2-L3					6 +- 3	-5 +- 1	-10 +- 2	3 +- 2	1 +- 1	-1 +- 1
	L3-L4					5 +- 3	-5 +- 3	-12 +- 1	1 +- 1	2 +- 1	-1 +- 1
	L4-L5					2 +- 3	-3 +- 2	-13 +- 4	2 +- 1	2 +- 1	-1 +- 1
(78)	L4-L5			6.1 (right) 6.9 (left)		0.9		14.3		0.6	
	L5-S1			4.5 (right) 4.8 (left)		0		10.2		0.2	
(30)	L1-L2	Range of motion during maximum lateral bending of 25°				4.7		2		0	
	L2-L3					6.25		2.1		2.2	
	L3-L4					6.13		1.3		3.8	
	L4-L5					4.53		1.9		2.8	
	L5-S1					3.39		-1		1	
(79)	1 L1-L2	Lab A				4.45		5.75		2.22	
	2 L1-L2					5.75		7.05		2.4	
	3 L1-L2					6.62		4.37		1.4	
	4 L1-L2					5.12		5.37		2.8	
	5 L1-L2					10.75		8.5		3	
	6 L1-L2					11.25		9		4	
	L3-L4					8.37		7.62		2.68	

1 L1-L2					5.37	5.25	2.09
2 L1-L2					6.62	6	2.2
3 L1-L2					6.62	4.25	1.22
4 L1-L2	Lab B				5.37	5.25	1.5
5 L1-L2					14.75	8.5	3.95
6 L1-L2					1.75	12	3.31
L3-L4					9.5	8.95	2.4
1 L1-L2					4.37	3.87	2.95
2 L1-L2					5.95	6.37	3.68
3 L1-L2					6.87	4.5	1.13
4 L1-L2	Lab C				5.5	5.37	3.3
5 L1-L2					7.5	9.25	2.54
6 L1-L2					11	7.5	4.18
L3-L4					9.25	7.5	3.36
1 L1-L2					4.55	6.18	2.81
2 L1-L2					6.37	5.75	3.68
3 L1-L2					5.75	3	3.25
4 L1-L2	Lab D				5.75	5.25	3
5 L1-L2					11.75	10	2.81
6 L1-L2					14	10.5	4.81
L3-L4					9.2	6.95	3.2

Appendix B – Intervertebral Disc Degenerated

Due to the morphologic changes, the motion of the lumbar spine is affected. Some papers studied the effect of different stages of the intervertebral disc degeneration on biomechanical behavior of a lumbar spine (67) (68) (69). The Table 2 summarizes the motion measured by the papers referenced anteriorly.

Table 2 - Summary of the lumbar spine motion with intervertebral disc degeneration during several movements: axial rotation, lateral bending, flexion and extension

Reference	Gender	Movement	Normal	Degeneration stage		
				III	IV	V
(69)	Male	Axial rotation	2.2	4.4	6.1	5.1
		Lateral Bending	7.2	10.4	8.9	8.4
		Flexion	2.8	4.3	4.8	3.8
		Extension	2.3	2.7	3.4	3
	Female	Axial rotation	3.6	5.2	7.5	6.6
		Lateral Bending	11	13	12	9.4
		Flexion	4.7	5.5	6.2	5.2
		Extension	3.3	3.5	4.9	3.1
(68)	-	Flexion	45.1	42.4	50.6	41.5
		Extension	13.7	9.5	7.4	12.8
		Right lat. Bend.	24.4	20.8	24.4	19.2
		Left lat. Bend.	23.9	23.9	23.2	21.8
		Right ax. Rot.	15.3	15	17.3	17.2
		Left ax. Rot.	17	16.5	18.2	16.4
(67)	-	Flexion/ extension	12.25	12	10.6	8.5
		Lateral Bending	11.1	9.5	7.8	2.4
		Axial rotation	2.4	2.9	3.8	2.5

Interpreting the Table 2 it was possible to conclude that during the axial rotation, the rotation increases with the stages of the degenerative disc, reaching the maximum at stage IV, and then the rotation decreases a little, being higher than the normal rotation (for the right axial rotation) and smaller than the normal rotation (for the left axial rotation). For the lateral bending, the rotation increases reaching the maximum value at stage III, then it decreases progressively reaching values smaller than the normal motion at stage V (for both sides). During the flexion, it is not very clear how

the motion behaves with the different stages, because two measurements show that the rotation increases, reaching the maximum at stage IV and then decreases to values that is higher than the normal rotation. On the other hand, the two other measurements shows that the rotation decreases at stage III, following of an increase, where it reaches the maximum value, and then decreases again to values smaller than the normal motion. For the extension, the same happens because the results are not concordant. From one paper, it shows that the motion increases until reaching the maximum at stage IV, and then decreases to values higher than the normal motion, for females, and smaller than the normal motion for males. On the others hands, the second paper shows that the motion always decreases until the stage IV, and then increase, but the value is smaller than the normal motion.